NextGEM

Next Generation Integrated Sensing and Analytical System for Monitoring and Assessing Radiofrequency Electromagnetic Field Exposure and Health

D4.7: Technical report on the results on dosimetry - Final report

Document Summary Information

Start Date	01/07/2022	**Duration**	48 months
Project URL	https://www.nextgem.eu/		
Deliverable	D4.7: Technical report on the results on dosimetry - Final report		
Work Package	WP4	**Task**	T4.2
Contractual due date	30/11/2024	**Actual submission date**	29/11/2024
Type	Report	**Dissemination Level**	PU-Public
Lead Beneficiary	UCAS	**Deliverable Editor**	Fulvio Schettino (UCAS)

This project has received funding from the European Union's Horizon Europe research and innovation programme under the Grant Agreement No 101057527

Contributors and Peer Reviewers

Contributors
Marco Spirito (TUD), Maryse Ledent and Seppe Segers (SC), Benjamin Vatovez (ISSeP – Subcontractor SC), Olga Zeni and Stefania Romeo (CNR), Fulvio Schettino, Mario Lucido and Marco Donald Migliore (UCAS), Erdal Korkmaz (THUAS), Anna Bogdanova (UZH), Yuri Feldman and Igal Bilik (HUJI), Anna Laromaine, Marti Gich, Pol Alonso (CSIC), Mathieu Pruppers (RIVM), Francisco Vargas Marcos (MHS), Nikolaos Petroulakis (FORTH), Eduardo Soudah (CIMNE)
Peer Reviewers
Yuri Feldman (HUJI), Olga Zeni (CNR)

Revision history (including peer-reviewing and quality control)

Version	Issue Date	Changes	Contributor(s)
v0.1	1/09/2024	Table of Contents provided	Fulvio Schettino (UCAS)
v0.2	1/09/2024	Sections populated with the Task leaders	Fulvio Schettino (UCAS)
v0.3	1/10/2024	Section defined, assigned, and agreed	Fulvio Schettino (UCAS)
v0.4	25/10/2024	First contributions	All partners
v0.5	05/11/2024	Integration and harmonization	Fulvio Schettino (UCAS)
v0.6	15/11/2024	Second contributions and updates	All partners
v0.7	18/11/2024	Complete version ready for peer review	Fulvio Schettino (UCAS)
v0.8	22/11/2024	Peer review	Olga Zeni (CNR) and Yuri Feldman (HUJI)
v0.9	27/11/2024	Comments addressed from peer review, technical and quality assurance	Mats-Olof Mattsson (SPi), Nicolas Louca (EBOS)
v1.0	29/11/2024	Final review and submission	Nikolaos Petroulakis (FORTH)

Disclaimer

Funded by the European Union. Views and opinions expressed are however those of the author(s) only and do not necessarily reflect those of the Euro pean Union or the European Commission. Neither the European Union nor the granting authority can be held responsible for them."

Copyright message

Table of Contents

List of Figures

List of Tables

Glossary of terms and abbreviations used

Abbreviation / Term	Description
BL	Bottom Layer
CV	Coefficient of Variation
DMEM	Dulbecco's Modified Eagle Medium
DUT	Device Under Test
ELF	Extremely Low Frequency
EM	ElectroMagnetic
EMF	Electromagnetic Fields
ERP	Ear Reference Point
FDTD	Finite-difference time-domain
FR1/FR2	Frequency Range 1/2
GA	Grant Agreement
GLP	Good Laboratory Practice
ICES	International Committee on Electromagnetic Safety
ICF	Informed Consent Form
ICNIRP	International Commission on Non-Ionizing Radiation Protection
IEEE	Institution of Electrical and Electronic Engineers
IF	Intermediate Frequency
IPD	Incident Power Density
LUT	Look up Table
MF	Magnetic Field
NGM	Nematode Growth Medium
PEC	Perfect Electric Conductor
RBC	Red Blood Cells
RC	Reverberation Chamber
RFM	Rational Function Model
ROI	Region of Interest

SAR	Specific Absorption Rate
SH-SY5Y	Human neuroblastoma cell line
SUT	Sample Under Test
TRL	Thru-Reflection-Load
VNA	Vector Network Analyzer
WG	Waveguide
WP	Work Package
WS	Whole Sample

Executive Summary

Deliverable D4.7 "Technical report on the results on dosimetry - Final report" is part of Work Package (WP) 4 and provides the technical details of all the exposure systems to be used for biological experiments within the NextGEM project. It represents an update of D4.2, and is released at the end of Task 4.2 activity. The main goal is to create a solid technical ground for all the experimental activities envisaged in WP4, including numerical and experimental dosimetry. Each exposure system setup is presented, including a technical description, and validated by means of thorough numerical dosimetry, if currently available: the dose homogeneity is a guiding design principle and an aspect of paramount importance for establishing a link between the exposure and the possible effect, according to the recommendations for Good Laboratory Practice (GLP). An important contribution of this document is to ensure that all the experimental studies (*in vitro*, *in vivo* and *ex vivo*) within the NextGEM project comply with GLP. A dosimetry analysis to estimate the Specific Absorption Rate (SAR) levels on buccal cells from heavy and light mobile phone users is also planned during the project: the initial activity of setting up the related suitable models is reported in this document. Finally, as part of the process to achieve a correct dosimetry evaluation, the electromagnetic characterization of the materials involved in the experimental studies, such as culture media, is also covered in this document. Models and methods are reported, as well as the results of the measurements carried out during the first part of the project.

1 Introduction

While emerging technologies in telecommunications are profoundly and rapidly changing the way of people´s life, the increasingly pervasive use of radiofrequency (RF) electromagnetic fields (EMF) is raising concerns in some citizen groups, perceiving EMF as a threat to public health. The exposure standards for workers and for the general public, issued by the International Commission on Non-Ionizing Radiation Protection (ICNIRP) and the International Committee on Electromagnetic Safety of the Institute of Electrical and Electronic Engineers (ICES-IEEE), are set to prevent the occurrence of adverse health effects and are based on comprehensive reviews of the relevant scientific literature. Anyway, technical knowledge and scientific literature must be continuously fed by high-quality research because technology advances rapidly, and new concerns are expected to arise.

The NextGEM project is placed in this context, aiming to collect robust and reliable data by combining different experimental approaches: *in vitro* studies on human cell lines, *in vivo* studies on the model organism *Caenorhabditis elegans* (*C. elegans*), and *ex vivo* studies on human cells. For the experimental activity to be reliable, it must be quality-driven, according to the recommendations for GLP. Exposure systems for biological experiments have to be designed, characterized and optimized resorting to a thorough numerical and experimental dosimetry, which is the accurate estimation of the dose effectively delivered to the bio-system. This is the only trustable way to establish a causal link between exposure and a substantiated effect, if any.

1.1 Mapping NextGEM Outputs

The purpose of this section is to map NextGEM's Grant Agreement (GA) commitments, both within the formal Task description and Deliverable, against the project's respective outputs and work performed.

Table 1: Adherence to NextGEM's GA Tasks and Deliverables Descriptions

TASKS	
Task Number & Title	**Respective extract from formal Task Description**
Task 4.2 - Exposure systems set up and dosimetry	GLP requires a careful design of exposure systems, considering SAR uniformity and power density. This task is devoted to the design and characterization of new exposure systems and optimization of existing ones to comply with the specific biological protocol and to the selected exposure conditions. Moreover, a thorough numerical dosimetry will be carried out in order to analyse the effect of the many design parameters on the dosimetry quantities (SAR, E field, energy density) in the sample in order to guarantee the desired homogeneity in dose distribution (by means of variation coefficient, i.e. ratio between standard deviation and average SAR). As the complex permittivity of involved materials is a fundamental parameter for a correct dosimetry, new online and offline measurement techniques will also be implemented, based on interferometric techniques to improve sensitivity. Specific exposure system and dosimetry analyses will be developed for the exposure of *C. elegans*.
DELIVERABLE	
Deliverable: D4.7: Technical report on the results on dosimetry - Final report (M29) This deliverable will provide a comprehensive final analysis of numerical dosimetry and optimization of exposure systems for bio-experiments.	

1.2 Deliverable overview and report structure

Based on the objectives and work carried out under Task 4.2, the document starts with the Executive Summary followed by the Introduction of the document in Section 1.

Sections 2 and Section 3 are devoted to the description of the exposure systems that will be used within the NextGEM project in the sub 6GHz band and in the millimetre-wave band respectively, and report the data related to the available dosimetry.

The aim of Section 4 is to describe numerical models and methods to be used to analyze the exposure of light and heavy mobile users.

Section 5 focuses on the electromagnetic characterization of materials, including the models and the measurement techniques, as well as the currently available results.

Finally, Section 6 concludes the deliverable.

1.3 Updates from previous Deliverable D4.2 "Technical report on the results on dosimetry– Initial version"

As already stated, this deliverable is a continuation and an update on the exposure systems design and characterization, to what has been detailed in D4.2 "Technical report on the results on dosimetry– Initial version". In fact, the numerical and experimental dosimetry of some exposure systems were already completed at the time of D4.2 submission, thus allowing experiments planned in the first part of the project to be carried out. This is the case of the systems described in Sections 2.1 and 3.2, which remain basically unchanged, as well as the methodological Sections 4 and 5, apart from some minor updates. The main additions to this deliverable can be summarized as follows:

- Section 2.2 has been completely rewritten, as the preliminary results of the initial design of the setup were unsatisfactory, not complying with the high quality standards envisaged within the NextGEM project. A completely different design has been now proposed, and the dosimetry presented.
- The system presented in Section 2.3 is basically unchanged in its working principle, but a different scenario of multiple frequency exposures has now been added: consequently, the change of the setup for this new scenario is presented in Section 2.3.2.2, and the related dosimetry has now been added in Section 2.3.3.2.
- Section 3.1 has now been fully populated with the description of the final design of the exposure setup (Section 3.1.2) and the related dosimetry (Section 3.1.3).

2 Exposure systems in the sub 6GHz band

Exposure systems design has to rely on different principles depending on the wavelength. While at higher frequencies the exposed sample is usually in the far field zone with respect to the radiating system (see D3.5 for a definition of far field and near field regions), this is not true at lower frequencies, thus implying completely different design approaches. For this reason, the exposure systems to be used within the NextGEM project have been grouped depending on the design frequency: in this section, the systems working at frequencies below 6GHz are listed, capable of employing signals compliant with 2G-4G standards as well as 5G in the Frequency Range 1 (FR1). As a general good practice, background fields (ELF and MF) have been checked in order to exclude any influence on the RF exposures.

2.1 Exposure system at Sciensano: sXc3500

2.1.1 Introduction

Sciensano utilizes the sXc3500 exposure system, acquired from the IT'IS Foundation, for the NextGEM project. This waveguide-based system is designed for *in vitro* cellular exposure at a frequency of 3.5 GHz, with various modulation options available. The system also enables blinded exposure to ensure experimental integrity.

This system is used in Task 4.3 to expose cell cultures (HaCaT cells, a human keratinocyte-derived immortalized cell line) to different exposure parameters with the goal of studying a variety of biological endpoints, including genotoxicity (micronucleus, alkaline comet assays), epigenetics, transcriptomics (TempO-Seq, qPCR), oxidative stress (colorimetric and fluorescent/luminescent assays), cell proliferation (flow cytometry, colorimetric/fluorescent assays) and apoptosis (flow cytometry, colorimetric/fluorescent assays). Additionally, a study is performed with human lymphocytes, which will be extracted from blood samples of volunteers. These cells are exposed *in vitro*. Afterwards, extracted cells is tested for genotoxicity (micronucleus test and comet assay) and RNA is extracted for use in transcriptomics experiments (qPCR on selected genes based on TempO-seq experiments in HaCaT).

The results of the dosimetric analysis for the sXc3500 presented in this deliverable were obtained by the IT'IS Foundation[1].

Figure 1: Pictures of the exposure system. The waveguides inside the incubator (left) and the signal tower including the vector signal generator and the amplifier (right).

2.1.2 Setup description

The sXc3500 exposure system (Figure 1) was developed based on the sXc1800 system described in [1], but changed to use 3500 MHz instead of 1800 MHz. The dosimetry of the sXc3500 system was assessed separately. The system was designed to produce RF-EMF exposures of fifth-generation (5G) mobile communication devices operating at

[1] https://itis.swiss/who-we-are/

3500MHz. A 256QAM modulated signal with a bandwidth of 100 MHz and a sub-carrier spacing of 60 kHz can be generated. The setup is based on two R32 rectangular waveguide chambers that are excited by a fully computer-controlled signal unit, allowing for blind exposure between the two waveguides, with one being actually exposed and the other one used for a sham control condition. The system is optimized to expose cell monolayers with minimum uncertainty, maximum uniformity, and well-defined temperature load. The system allows the exposure of six cell cultures hosted in 35 mm Petri dishes held in position by a tray. The tray is placed in an R32 waveguide fed by a coaxial to waveguide transition and closed by a short. The location of the short determines the position of the fields in the waveguide and is used as a reference for positioning other elements.

2.1.3 Numerical dosimetry

2.1.3.1 Exposure system model

The model used to calculate dosimetry can be found in Figure 2.

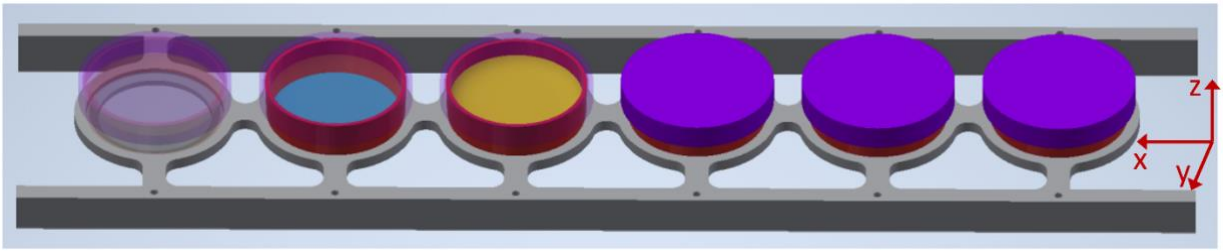

Figure 2: Geometry overview of the sXc3500 dish holder (gray), the 6 dishes (red), the lid (magenta), the monolayer (cyan) and the medium+meniscus (yellow)

The dishes are modelled as shown in Figure 3. Each sample consists of a cell monolayer settled down at the bottom of the culture dish. Medium volumes of 2.2, 2.8, 3.1, 3.4 and 4.0 mL are considered, which are in the range typically employed in biological experiments and allow to obtain a kind of system calibration as discussed in subsection 2.1.3.4. The monolayer height is always 200 μm. The dish and the medium+meniscus are angled as specified by the dish manufacturer (1.72°) to match the real dish profile.

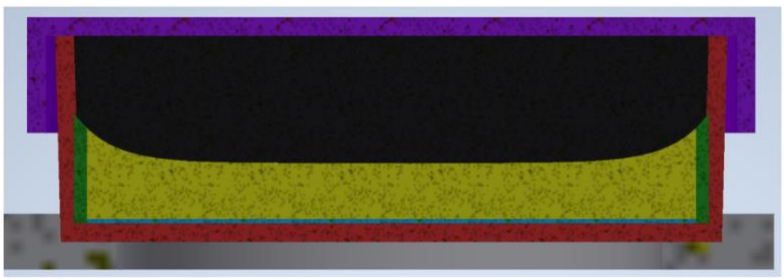

Figure 3: Detailed section view of the dish holder (gray), the dish (red), the lid (magenta), the monolayer (cyan), the medium+meniscus (yellow), and the filler (green).

The meniscus profile is modelled according to [2] using the parametric equation (1) expressing the height $h(r)$ above the level without meniscus as a function of the radius r. The equation is valid up to R_0, that is the radius of the medium cone at the final height, following the half-cone opening angle of 1.72°:

$$h(r) = h_0 \left(e^{\frac{R_0 - r}{c}} + e^{\frac{R_0 + r}{c}} \right), \|r\| \leq R_0 \quad (1)$$

with h_0 = 2.51 mm, c = 1.96 mm.

The life science simulation platform Sim4Life[2] (ZMT Zurich MedTech AG, Switzerland) was used to perform a numerical Finite-Difference Time-Domain (FDTD) analysis with the different medium volumes (2.2, 2.8, 3.1, 3.4 and 4.0 mL). All experiments were repeated with different voxel sizes to evaluate the voxeling uncertainty:

- **Mesh 0:** monolayer 0.025 x 0.025 x 0.025 mm; medium, meniscus and dishes 0.1 x 0.1 x 0.1 mm; elsewhere 0.1 x 0.1 x 0.1 mm

[2] https://zmt.swiss/sim4life/

- **Mesh 1:** monolayer 0.05 x 0.05 x 0.05 mm; medium, meniscus and dishes 0.2 x 0.2 x 0.2 mm; elsewhere 0.2 x 0.2 x 0.2 mm
- **Mesh 2:** monolayer 0.1 x 0.1 x 0.1 mm; medium, meniscus and dishes 0.5 x 0.5 x 0.5 mm; elsewhere 0.5 x 0.5 x 0.5 mm

The absorbed power extracted from the electromagnetic (EM) results was then used as a heat source in a thermal transient simulation (Pennes Bioheat equation model). The biofeatures (heat generation and heat perfusion) of the model are disabled. The thermal simulation is performed for the dish close to the short only, with the following voxel size: monolayer 0.2 x 0.2 x 0.1 mm, elsewhere 0.4 x 0.4 x 0.2 mm. The overall input power is normalized to a unit power of 1W. The simulation assumes transfer due to conduction, radiation, natural convection and forced convection by applying the following heat transfer coefficients based on literature values for similar materials and exposure conditions [1][2]: $h_{dish-air}$ = 41.1 W /Km² and $h_{medium-air}$ = 7.1 W /Km².

Simulation is repeated for the cooling case without a heat source.

Material parameters

The material parameters used for the EM and thermal simulations are defined in Table 2 and Table 3 respectively.

Table 2: EM parameters used for EM simulations at 3.5 GHz.

Item	Material	Relative Permitivity	Electric conductivity (S/m)
Waveguide boundaries except source	Perfect Electric Conductor (PEC)	-	∞
Tray and Petri dishes	Polystyrene	3	0
Medium	Dulbecco's Modified Eagle Medium (DMEM)	72	4,25

Table 3: Thermal parameters used for thermal simulations.

Item	Material	Specific Heat Capacity (J/kg/K)	Thermal conductivity (W/m²/kg)	Volumic mass (kg/m³)
Tray and Petri dishes	Polystyrene	1670	0,138	1200
Medium	DMEM	4148,3	0,563	1000

Definititions

For each dish *i*, the average Specific Absorption Rate (SAR) over the monolayer *i* is extracted from simulation data as $\langle SAR \rangle_i$ and standard deviation of the SAR over the monolayer *i* as $\sigma_{SAR,i}$. These parameters allow to define the local SAR non-uniformity, defined as the Coefficient of Variation (CV) for a given monolayer of dish *i* as in equation (2):

$$CV_i = \frac{\sigma_{SAR,i}}{\langle SAR \rangle_i} \tag{2}$$

The overall monolayer SAR non-uniformity CV is derived using equation (3). It is a generalization of equation (2), using the overall standard deviation and the mean of all monolayer SAR averages $\langle SAR \rangle_i$. The overall standard deviation is corrected for the variation of the mean for each monolayer *i*. The correction takes into account the number of voxels N_i in each monolayer *i*, N being the overall number of voxels:

$$CV = \sqrt{\frac{\sum_{i=1}^{6}(\sigma_{SAR,i}^2(N_i(\langle SAR \rangle - \langle SAR \rangle_i)^2)}{N-1}} * \frac{6}{\sum_{i=1}^{6}\langle SAR \rangle_i} \tag{3}$$

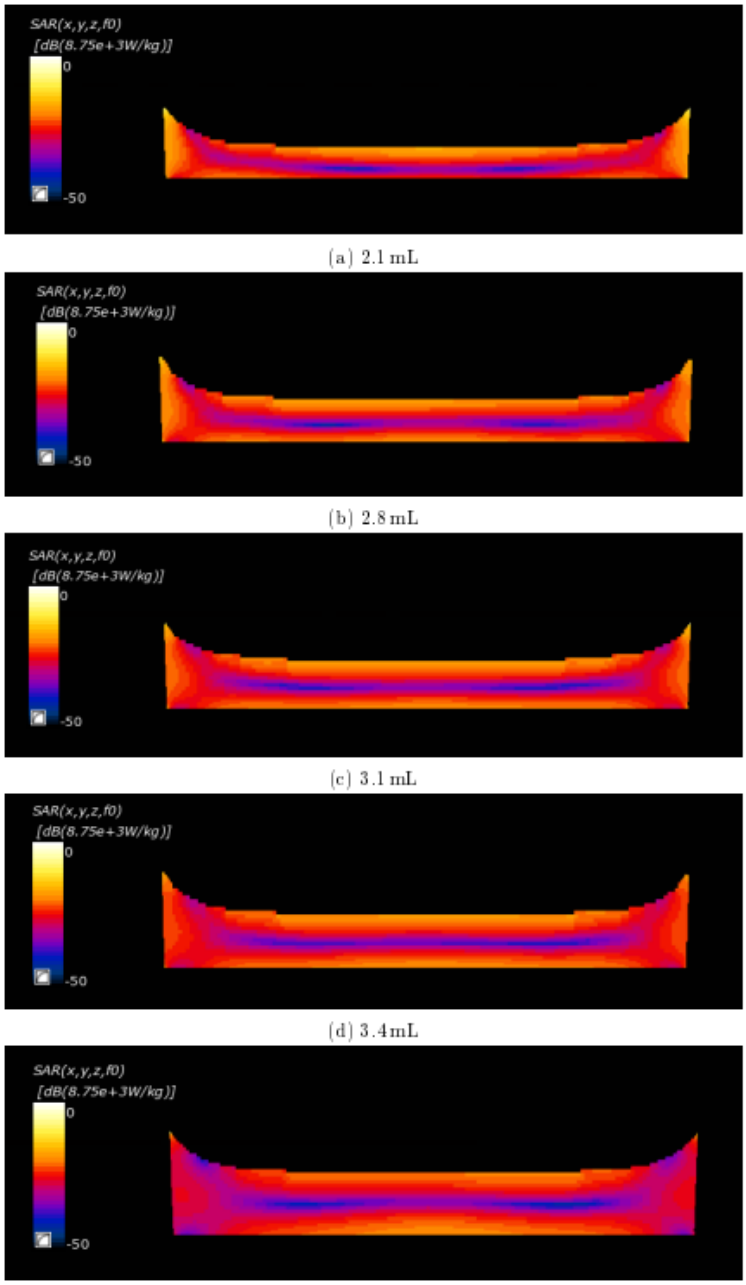

(a) 2.1 mL

(b) 2.8 mL

(c) 3.1 mL

(d) 3.4 mL

(e) 4.0 mL

Figure 4: Detailed view of SAR of dish 1, transverse plane XZ, using mesh 0 (-50 to 0 dB scale, with a dB reference at 8750W which was the maximum achieved SAR value, SAR for 1W input power).

2.1.3.2 SAR

SAR uniformity

A typical SAR profile for monolayer exposure is shown in Figure 4 in the plane XZ (see Figure 2). The liquid boundaries in this section are exposed to high SAR, while the core of the liquid experiences minimal SAR. Figure 4a to 4e show that as the volume in the dishes increases, the SAR profile along the monolayer (bottom of the dish) changes and a minimum occurs also at the corners in the X direction of the bottom monolayer. All considerations on non-uniformity are confirmed numerically (Table 4). Therefore, a volume of 3.1 mL is preferable for better uniformity and will be used in the biological experiments.

Statistics

The overall SAR statistics for mesh 0 are reported in Table 4.

Table 4: Monolayer dosimetry data for the sXc3500 system, mesh 0.

Medium volume of numerical model (mL)	2,1	2,8	3,1	3,4	4
Average SAR [W/kg/(A/m)²ref/(S/m)]	1,88	3,09	4,57	7,31	20,68
SAR nonuniformity CV (%)	61,19	37,93	29,88	33,98	40,28

Table 5: Monolayer SAR average and non-uniformity for all dishes.

SAR [W/kg] (non-unif. [%])	2,2 mL	2,8 mL	3,1 mL	3,4 mL	4,0 mL
Monolayer 1	1,59 (54,28%)	2,99 (35,80%)	4,51 (31,25%)	7,24 (33,60%)	16,47 (39,04%)
Monolayer 2	1,91 (56,62%)	3,04 (37,38%)	4,47 (29,74 %)	7,20 (32,54%)	16,91 (39,15%)
Monolayer 3	2,14 (58,70%)	3,09 (39,06%)	4,46 (29, 11%)	7,17 (32,72%)	17,98 (38,28%)
Monolayer 4	2,15 (60,29%)	3,12 (39,37%)	4,52 (28,89%)	7,23 (33,41%)	20,09 (35,11%)
Monolayer 5	1,93 (61,75%)	3,14 (38,33%)	4,64 (28,09%)	7,39 (34,34%)	23,66 (30,60%)
Monolayer 6	1,54 (63,91%)	3,15 (37,05%)	4,80 (30,31%)	7,63 (36,32%)	28,96 (27,75%)
Overall	1,88 (61,19%)	3,09 (37,93%)	4,57 (29,88%)	7,31 (33,98%)	20,68 (40,28%)

The SAR values are provided in Table 5. The best performance in terms of SAR non-uniformity is achieved for 3.1 mL loading of the dishes.

2.1.3.3 Thermal behavior

Thermal simulation data for the monolayer was fitted to exponential functions (4) and (5) to extract the parameters τ_{on} (rise time) and τ_{off} (fall time). Once the fitting parameters a, b, c, d have been calculated, it is possible to compute the heating ratio h defined by (6) from the a coefficient, linking the temperature increase to the monolayer SAR. Values are reported in Table 6.

$$f_1(t) = a\left(1 - e^{-\frac{t}{\tau_{on}}}\right) + b \tag{4}$$

$$f_2(t) = c\, e^{-\frac{t}{\tau_{off}}} + d \tag{5}$$

$$h = a\rho_{monolayer}\frac{SAR_{monolayer}\, V_{monolayer} + SAR_{medium} V_{medium}}{SAR_{monolayer}} \tag{6}$$

Table 6: Thermal figures of the monolayer for two medium volumes.

Medium volume of numerical model (mL)	3,1	4
τ_{on} [s]	271,33	261,04
τ_{off} [s]	300,74	305,11
h [°C/(W/kg)]	0,0718	0,0729

2.1.3.4 Dosimetry functions

The sXc exposure systems rely on a set of dosimetry functions to operate, depending on the specific dosimetry conditions. This section details the functions used for the new sXc3500 system which will operate for cell monolayer exposure only, which is of interest for the current project; different exposure conditions such as suspension exposure, require a separate dosimetry, not shown here. The parameters to be inferred from the cell volume are:

- average monolayer SAR as a function of the H-field value and the medium conductivity. The H-field value is measured by means of a monopole suitably located at the bottom of the waveguide at an E-field maximum to ensure a high signal-to-noise ratio;
- the average monolayer SAR non-uniformity;
- the average medium SAR. This value is necessary to extract the temperature increase in the cell medium.

Target SAR for monolayer

It is possible to derive a polynomial with coefficients p_1, p_2, p_3 expressing the monolayer averaged SAR as a function of cell medium volume:

$$SAR_{monolayer} = \sigma H^2 f^2 (p_1 + p_2 V_{medium} + p_3 V_{medium}^2) \quad (7)$$

where σ is the conductivity of the used cell medium in S/m, H^2 is the square of the H-field in A^2/m^2 as measured and calculated from the voltage output of the HF-detector, f is the frequency in Hz, and V_{medium} is the volume of the cell medium in mL. The parameters of the above-mentioned polynomial are reported in Table 7.

Table 7: Parameters for calculating monolayer average SAR according to medium volume.

p_1	p_2	p_3
2,3027 · 10^{-17}	-1,8027 · 10^{-17}	3,6067 · 10^{-18}

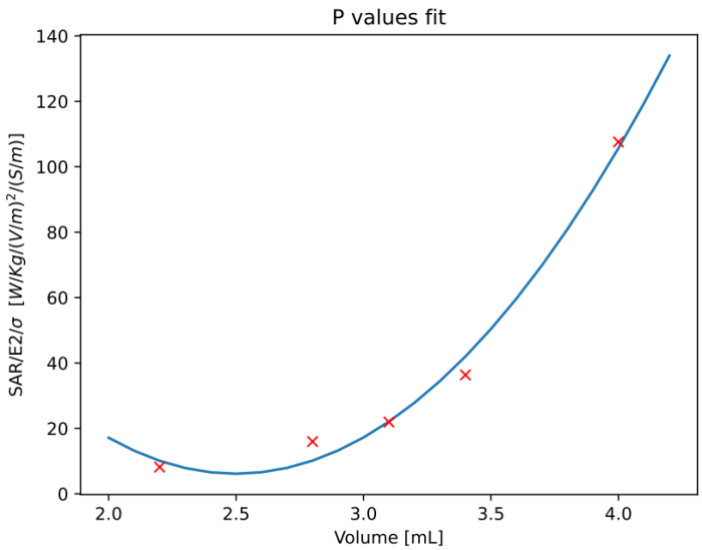

Figure 5: Monolayer SAR as a function of the cell medium volume, normalized to the square of E-field and to the conductivity.

Target SAR for whole medium

It is possible to derive a polynomial with coefficients d_1, d_2, d_3 expressing the whole medium averaged SAR as a function of the cell medium volume:

$$SAR_{medium} = \sigma H^2 f^2 (d_1 + d_2 V_{medium} + d_3 V_{medium}^2) \quad (8)$$

where σ, H, f and V_{medium} are defined as in (7). In this case, the value is not used directly for exposure but to compute the thermal load on the setup. This value cannot be used for exposure of cells grown in suspension. Its sole purpose is to assess the whole medium thermal load during monolayer configuration only (dishes in H-field maxima). The parameters of the above-mentioned polynomial are reported in Table 8.

Table 8: Parameters for calculating medium average SAR according to medium volume.

d_1	d_2	d_3
1,1788 · 10^{-17}	-9,1210 · 10^{-18}	1,8180 · 10^{-18}

SAR monolayer non-uniformity

It is possible to derive a polynomial with coefficient g_1, ..., g_4 expressing the monolayer SAR non-uniformity as a function of the cell medium volume:

$$CV\ [\%] = g_1 + g_2\, V_{medium} + g_3\, V_{medium}^2 + g_4\, V_{medium}^3 \tag{9}$$

where σ, H, f and V_{medium} are defined as in (7). The parameters of the above-mentioned polynomial are reported in Table 9.

Table 9: Parameters for calculating monolayer SAR non-uniformity according to medium volume.

Setup	g_1	g_2	g_3	g_4
sXc3500	285.72	-152.29	22.77	0

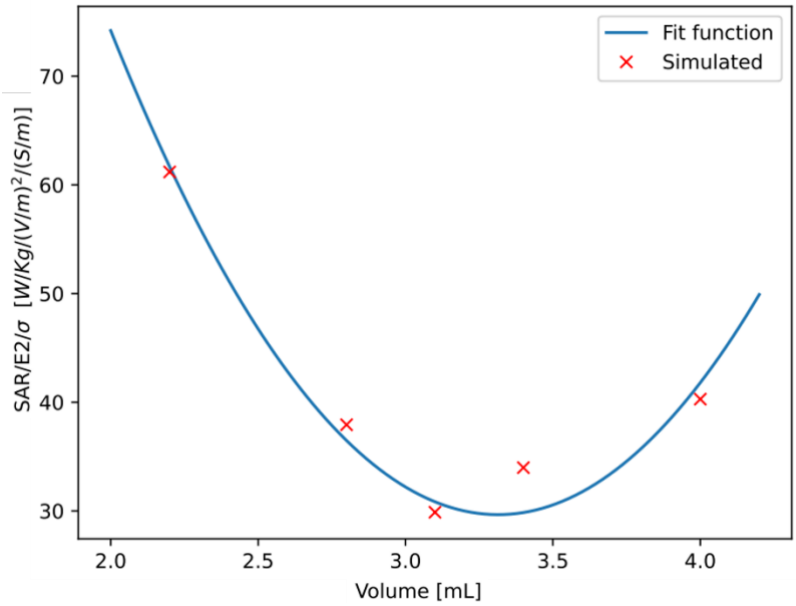

Figure 6: SAR non-uniformity as a function of the cell medium volume, normalized to the square of E-field and to the conductivity.

2.2 Exposure systems at University of Zurich and at Hebrew University of Jerusalem

2.2.1 Introduction

The exposure system described in this section was designed for blood exposure to the RF-EMF. It is used in Task 4.1 to assess the characteristics of red blood cells in flow under conditions of transient repetitive exposure to the RF-EMF, simulating the *in vivo* exposure scenario when using a cell phone.

2.2.2 Setup description

A novel exposure system in which blood (or any other liquid) samples can be exposed when flowing has been proposed and designed by HUJI. Currently, two prototypes are available, one at the HUJI premises and the other at the UZH premises. The key element is a thermostat-controlled cuvette with a system ensuring the liquid flow, exposed to EMF by a patch omnidirectional antenna connected to a generator, which is put in the special chamber; the case is coated with the RF absorbing material and shielded by the grounded metal plates. In more detail, the exposure chamber for both prototypes includes (Figure 7):

1. cuvette for RF exposure in which the volume of liquid remains constant during exposure (2.65 ml),
2. patch antenna connected to a generator,
3. RF Absorbing Material (WAVASORB),
4. metal plates (right).

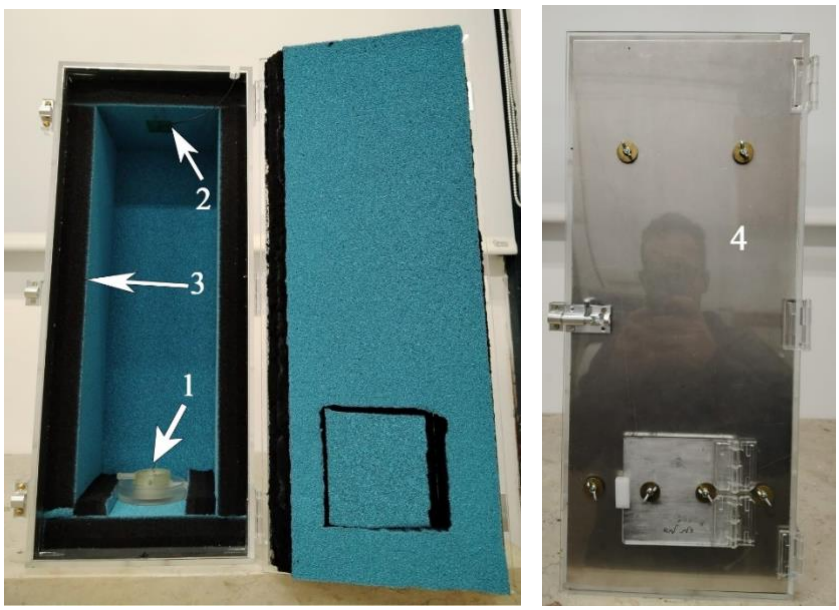

Figure 7: The exposure part of the proposed setup.

Different flow rates (1-20 ml/min) were tested, in a temperature range from 20-37°C at 1-6 GHz, 10 dBm with and without modulation protocols. The flow rate, cuvette filling, and cuvette temperature are computer-controlled. In particular the temperature is controlled by means of a thermocouple in the water jacket surrounding the cuvette, and thermostabilised by means of a Julabo thermostate with an accuracy of ±0.5°C After all the tests, the final flow rate in the exposure setup system at UZH was fixed to 9 ml/min. This value was chosen to mimic the flow of Red Blood Cells (RBCs) in blood vessels as closely as possible (although it is quite variable and dependent on vessel diameter, localization of the vessel, vascular tone, cardiac function, ambient temperature, and many other factors including weight and age). Blood flow in the capillaries is usually slower due to the smaller diameter and, hence, presents higher resistance and makes 0.5-1 mm/sec. The selected settings are comparable to the average blood flow rate that may be observed in humans [3]. The attenuation level was also tested using both transmitting and receiving antennas (the receiving antenna was put outside the closed chamber), and the result showed a level of about - 20 dB.

2.2.3 Numerical dosimetry

The numerical dosimetry was carried out by HUJI using the software CST Microwave Studio[3]. Some preliminary results are reported in the following. Figure 8 shows the model used to calculate dosimetry and the sample dimensions are shown in Figure 9.

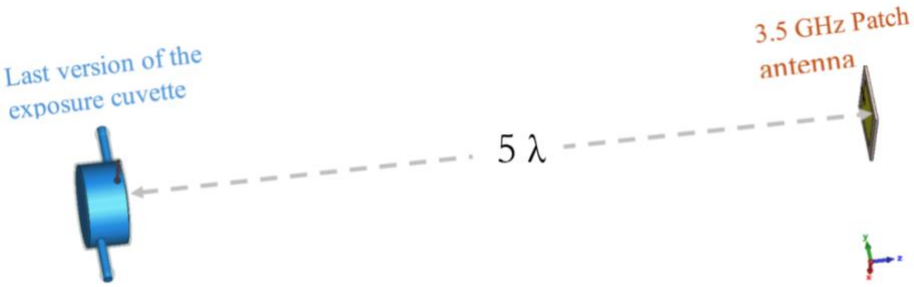

Figure 8: Relative position of the exposure cuvette and antenna.

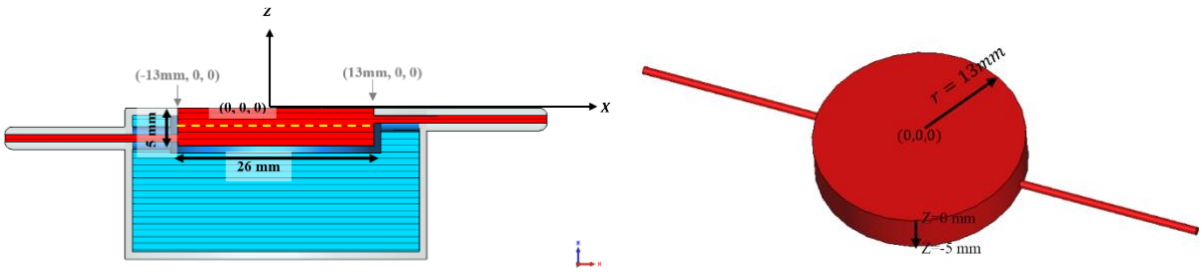

Figure 9: Sample geometry in the exposure cuvette.

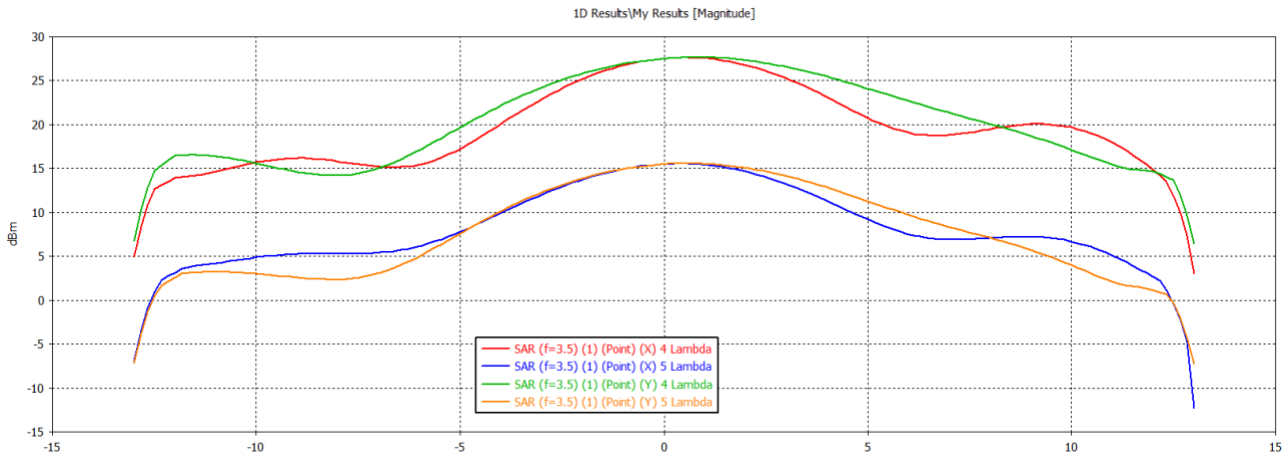

Figure 10: SAR distribution for the frequency 3.5 GHz for different axes and different relative positions (4λ and 5λ).

The SAR levels were mapped to the input power to confirm experimental setup validity. The CV values were compared for 4λ and 5λ distances between the antenna and the sample's brim, and the SAR distribution over the bandwidth of 50 MHz - (3.475, 3.525) GHz has also been checked. An average input power of 0.5 W was considered. The following sample parameters were taken into account $\Delta\,\varepsilon = 49.09$, $\tau = 6.94{\cdot}10^{-12}\ s$, $\alpha = 1 - 0.979$, $\varepsilon_\infty = 4.7$, $\sigma = 1.11\ S/m$, which were obtained by using Cole-Cole parameters measured by PNA at HUJI laboratory at 37 $°C$ (body core temperature). A water jacket at 37 $°C$ to emulate the temperature control in our system was also created using Cole-Cole parameters measured in our laboratory with the following values: $\Delta\varepsilon = 72.3$, $\tau =$

[3] https://www.3ds.com/products/simulia/cst-studio-suite

$6.27{\cdot}10^{-12}\ s$, $\alpha = 0$, $\varepsilon_\infty = 2.74$, $\sigma = 2.2{\cdot}10^{-8}\ S/m$. The results of the statistics are presented in Figure 10 and Table 10. Increasing the distance of the antenna from the sample from 4 λ to 5 λ, shows the increase of the CV by ~3%.

Table 10: Results of the statistical analysis.

EM Source	Average SAR (W/Kg)		SD (W/Kg)		CV	
	4 λ	5 λ	4 λ	5 λ	4 λ	5 λ
Reference patch antenna	0.0078	0.0019	0.0047	0.0012	60.7%	63.71%

Compared to the distributions obtained with 4 λ, these are similarly distributed in both x and y directions and more uniform (although the CV is higher by ~3%). The SAR distributions along the x and y axis (z= -2.5 mm) for the bandwidth of 50 MHz - (3.475 , 3.525) GHz with the center frequency of 3.5 GHz is shown in Figure 11. As it can be seen, the SAR distribution does not change over the bandwidth.

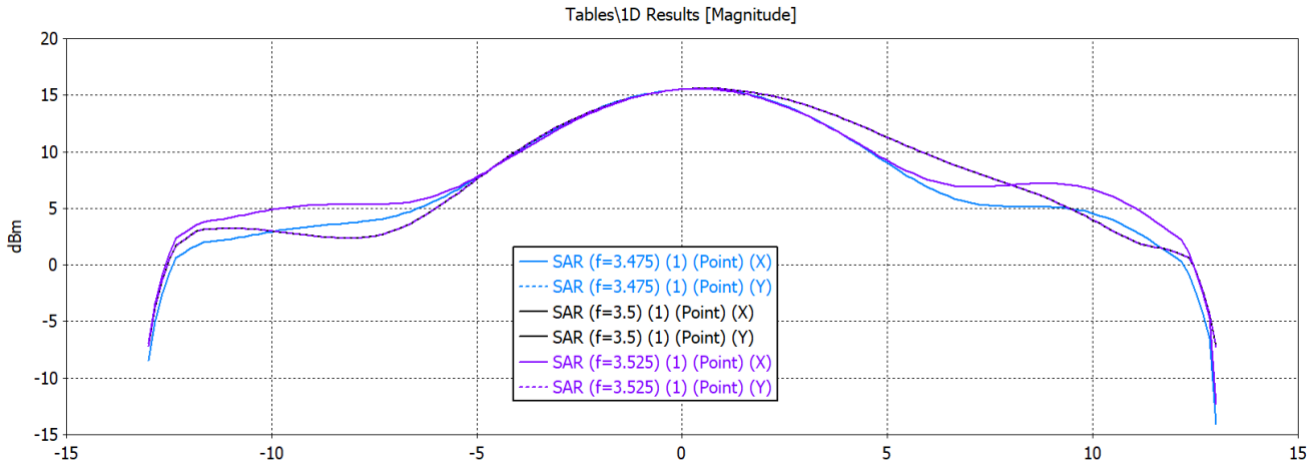

Figure 11: SAR distribution over the bandwidth of 50 MHz - (3.475 , 3.525) GHz with the center frequency 3.5 GHz.

Numerical dosimetry is currently being completed, after the selection of the final patch antenna to be used during the experiments. Nevertheless, the results reported in Table 10 give an idea of the order of magnitude of achievable SAR levels to be used in Case Studies foreseen within the NextGEM project.

2.3 Exposure system at CNR

2.3.1 Introduction

The CNR exposure system working in the sub 6 GHz band is based on short-circuited waveguides hosted in a standard cell culture incubator and allows exposure of cell cultures under strictly controlled conditions in terms of temperature and EM parameters. In particular, two set-ups have been realized and characterized to operate at either a single frequency EMF (1950 MHz) or at multiple frequencies (1800, 1950 and 2450 MHz), given simultaneously or in sequence. Within NextGEM, these set-ups will be used to expose/sham expose up to four samples of human neuroblastoma (SH-SY5Y) cells under the following conditions:

- Single frequency/single signal scenario (1950 MHz, 4G LTE signal, 1.25 and 0.3 W/kg SAR);
- Double frequency/double signal scenario (1950 MHz, 4G/LTE, and 2450 MHz, IEEE 802.11ax, RF-EMF, at 1.25 and 0.3 W/kg SAR, simultaneously).

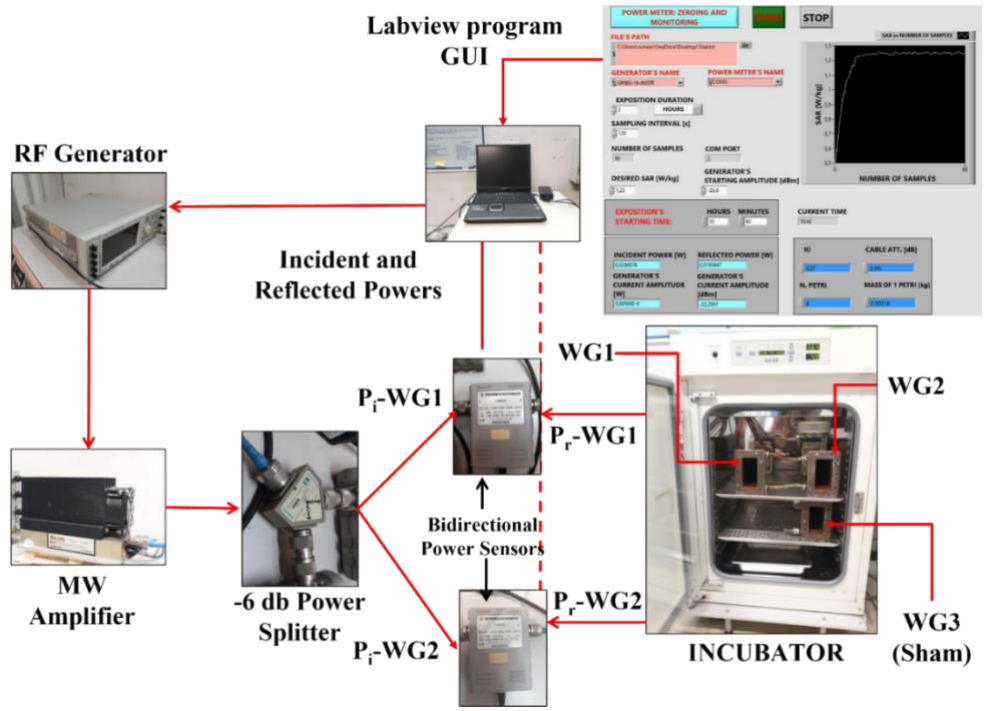

Figure 12: Configuration and components of the setup employed to expose cell cultures to single frequency EMF (GUI, graphic user interface; P_i, incident power; P_r, reflected power; WG, waveguide) [4].

2.3.2 Setup description

2.3.2.1 Single frequency/signal exposure scenario

The set-up configuration for the single-frequency exposure condition is sketched in Figure 12. The signal is provided by a RF generator (E4432B ESG-D, Agilent, Santa Clara, CA), sent to an amplifier (AM38A-0925-40-43; microwave amplifier, Bristol, England), and then to a -6 dB power splitter (HP11667A, Hewlett-Packard, Palo Alto, CA). In this way, two identical signals are obtained and sent through a couple of bidirectional power sensors (NRT-Z43, Rohde & Schwarz, Munich, Germany), to two identical RF applicators consisting of rectangular, short-circuited waveguides (WG, WR430, 350 mm long, SAIREM, Neyron, France), connected to the feeding side by means of a coaxial-to-waveguide adapter (Maury Microwave R213A2, VSWR: 1.05, Montclair, CA). Both the signal generator (via GPIB interface) and the power sensors (via USB interface) are remotely controlled in a feedback loop by means of a Labview (National Instruments, Austin, TX, USA) program that is employed to set the exposure parameters (frequency, desired SAR, exposure duration, and initial time of exposure), to continuously monitor the incident and reflected power levels, and to adjust them to keep the desired SAR constant throughout the whole exposure period. The two waveguides are placed inside a standard incubator (Forma Scientific, model 311) to guarantee environmental conditions suitable for cell cultures (37°C, 95% air, and 5% CO2 atmosphere). A third, identical waveguide, disconnected from the RF feeding and used for sham-exposures, is placed in the same incubator. Up to four samples (35mm Petri dishes) can be exposed simultaneously in each waveguide [4][5].

2.3.2.2 Multiple frequency/signal exposure scenario

The set-up configuration for simultaneous exposures to 1950 and 2450 MHz is shown in Figure 13 and represents an optimization of the setup presented in [8] and in D4.2. The 1950 MHz, 4G/LTE, and the 2450 MHz, WiFi (IEEE 802.11ax) signals are provided by an E4432B ESG-D (Agilent, Santa Clara, CA) and an SMM100A (Rohde&Schwarz, Munich, Germany) RF generators, respectively. Both signals are conveyed to a PD2020 (InNSTOCK wireless components, NJ, USA) power combiner, and the output signal is sent to an amplifier (AM38A-0925-40-43; microwave amplifier, Bristol, England), and then, through a bidirectional power sensor (NRT-Z43, Rohde & Schwarz, Munich, Germany), to a WR430 (350 mm long, SAIREM, Neyron, France) rectangular, short-circuited waveguide connected to the feeding side by means of a coaxial-to-waveguide adapter (Maury Microwave R213A2, VSWR: 1.05, Montclair, CA). The waveguide is placed inside a standard incubator (Forma Scientific, model 311) to guarantee environmental conditions suitable for cell cultures (37°C, 95% air, and 5% CO2 atmosphere), together with a second, identical waveguide, disconnected from the RF feeding and used for sham-exposures. Up to four samples can be exposed simultaneously in each waveguide. Customized, 30 mm diameter Pyrex dishes were used for cell cultures, which allowed the reduction of the non-uniformity degree to an acceptable level in the case of 2450 MHz [8], which is below 40%. The suitability of customized Pyrex dishes in

hosting SH-SY5Y cell cultures for RF exposures was assessed by performing a comparison between cell growth curves in customized dishes and in standard, 35 mm Petri dishes.

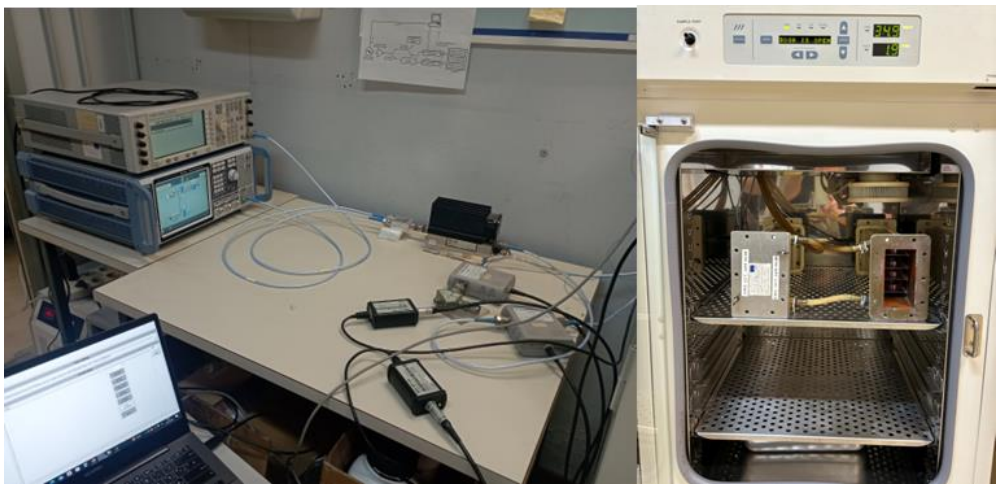

Figure 13: Configuration and components of the setup employed for simultaneous exposures of four samples to 1950 and 2450 MHz RF-EMF.

2.3.3 Numerical dosimetry

Numerical dosimetry analysis was carried out to identify the waveguide configuration and sample aspect that maximize the efficiency and uniformity of electric field (and SAR) distribution in the biological samples exposed to both single and multiple frequency scenarios. The methods and results of these analyses have been described in detail in our previous papers [6][7][8], and are briefly recalled in the following. The average SAR over the sample per unit of incident power (Watt per kilogram/Watt), was calculated as an indicator of the average specific efficiency. The Coefficient of Variation (CV), defined as the standard deviation of the SAR over the mean value, was adopted as an indicator of the SAR non-uniformity degree (see equation (2)). The overall efficiency (ratio between the absorbed and incident powers) was also reported. Both the efficiency and SAR homogeneity depend on the sample position with respect to the short circuit. Thus, the adopted approach was to pursue the best trade-off between the two parameters, considering that an acceptable value for the CV is about 0.3.

As a follow-up of the analysis described in D4.2 for *in vitro* exposures to multiple frequency/signal scenario in the FR1 band, numerical and experimental dosimetry were carried out to improve the set-up described in the initial report to optimize homogeneity of SAR distribution in the exposed samples. The final aim was to expose four samples to 1950 MHz, 4G/LTE, and 2450 MHz, IEEE 802.11ax, RF-EMF, at 1.25 and 0.3 W/kg SAR, simultaneously.

2.3.3.1 Single frequency/signal exposure scenario

Simulations were run in the CST Microwave Studio environment. The rectangular waveguide (inner transversal dimensions: 109.2 mm × 54.6 mm) was modelled as perfectly conductive with the longitudinal axis and narrow side horizontal, to achieve the condition of an unperturbed (empty waveguide) E vector parallel to the sample layer. The system was first simulated at 1950 MHz [6][7]. The four samples were modelled as cylinders (34 mm diameter, 3.3 mm thickness), with EM properties of cell culture medium (DMEM relative permittivity, $\varepsilon_r = 75$, effective conductivity, $\sigma = 2.2$ S/m, and mass density, $\varrho = 1060$ kg/m3), placed inside four polystyrene ($\varepsilon_r = 2.6$), 35 mm Petri dishes and located on a four-layer Plexiglas stand. It was demonstrated that, under the TE_{10} propagation mode, by placing the sample centers at a distance of $0.56*\lambda_z$ from the short-circuit, the efficiency of the exposure system was approximately 70%, and the CV of SAR distribution was 0.33 in all samples. Moreover, by exploiting the parabolic profile of the electric field in the waveguide cross-section, the vertical distance between samples was arranged in such a way to simultaneously expose two couples of samples to two different SAR values (ratio 1:4 between the central and the distal positions). The results of numerical analysis were confirmed by experimental dosimetry. The reliability of the calculated SAR and CV was checked by local temperature measurements with thermocouple (PT-6 Physitemp Instruments, kept perpendicular to the field) and fibre optic sensors (FISO Technologies) placed in different positions inside the Petri dish. The calculated overall efficiency was checked by measuring the amplitude of the reflection coefficient of the loaded waveguide applicator [6].
Similar analyses were performed to characterize the waveguide applicator for single-frequency exposures at 1800 MHz and 2450 MHz. At 1800 MHz, an overall efficiency of 56% and a CV of about 0.33 were achieved by locating the center of the sample at a distance of about $0.5*\lambda_z$ from the short circuit, whereas the condition in which two

samples were exposed to the same SAR or two couples of samples were simultaneously exposed to two different SAR values (ratio 4 or 2) was achieved by properly setting the vertical spacing between the inner samples and that between the outer and inner ones. In all cases, the overall efficiency was about 90%, and the CV was about 0.33 in both the inner and outer samples.

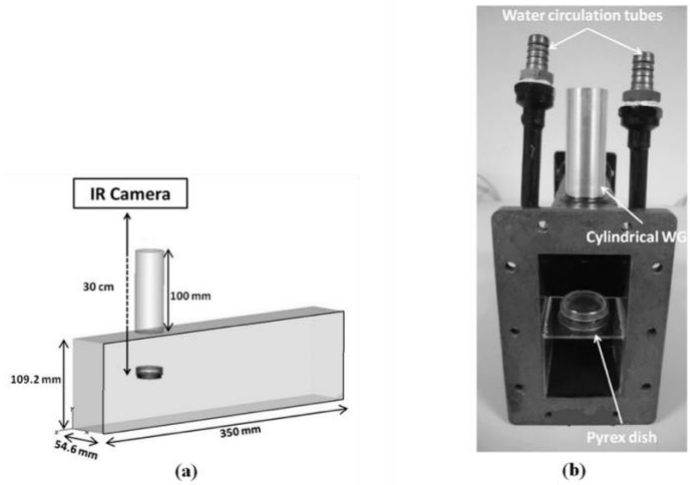

Figure 14: (a) Schematic model of the customized waveguide (WG) applicator adopted to perform calorimetric measurements. The position of the infrared (IR) camera is also indicated and (b) its realization loaded with a customized Pyrex dish hosted on a Plexiglass stand.

At 2450 MHz, it was not possible to find a scenario that fulfilled the established field uniformity requirements when using standard 35mm Petri dishes. This result was ascribable to the wavelength into the medium (λ_z = 17.6 mm), which is comparable to the radius of the Petri dish. Thus, the numerical analysis was replicated by gradually reducing the dish radius until an acceptable CV was achieved. This was obtained with a dish diameter of 30 mm, which resulted in the best trade-off between a good electric field uniformity and the possibility of hosting cell culture volumes sufficient to carry out most of the biological tests. Customized 30-mm Pyrex dishes were realized by a local manufacturer, and their suitability for cell cultures was checked by performing cell growth and viability assays [8].

Experimental dosimetry was carried out separately at 1800, 1950 and 2450 MHz by broadband measurements of the scattering parameters of the WG applicator. An Agilent E5071C network analyzer (9 kHz–4.5 GHz) was employed, and measurements of the loaded applicator were performed after Thru-Reflection-Load (TRL) calibration. Independent calibration procedures were performed before each measurement in a band centred at the frequency of interest. Calorimetric measurements were also carried out on a customized prototype of the applicator to assess electric field uniformity. A cylindrical waveguide (35 mm diameter, 100 mm length) was added on the short side of the WR430 guide at 140 mm from the short circuit, to allow optical inspection of the culture dish during the exposure. A schematic model of the exposure chamber is reported in Figure 14a, while a photograph of the WG applicator customized with the cylindrical guide and with a Pyrex dish located inside a Plexiglas stand is shown in Figure 14b. Calorimetric measurements were performed by means of an infrared camera (Thermovision A40, FLIR Systems, USA), which was used to measure the surface heating rate pattern in the medium during exposures to a high-power level. To perform a non-perturbing measurement, the camera was located at 30 cm from the sample, which was visible through the cylindrical WG. Temperature data were acquired over a time range of 120 s, with a 1 Hz sampling rate. Local temperatures were extracted by post-processing with the ThermaCAM Researcher PRO 2.8 SR-1 (FLIR System) software in a Region Of Interest (ROI) corresponding to the culture medium. The experimental setup adopted for these measurements was the same as the one described in section 2.3.2.1, except that only one power meter was employed. A quantitative comparison between simulated average SAR, the one achieved by calorimetric measurements, and the one obtained by power measurements is reported in Table 11. The agreement is satisfying, considering the accuracy of the thermal camera (2%), the unavoidable thermal drift affecting the detection of lower temperatures, and that the selection of the ROI for the assessment of the thermal distribution was performed by means of a freehand selection function from the image captured with the thermal camera [8].

2.3.3.2 Multiple frequency/signal exposure scenario

For the multiple frequency scenario, preliminary parametric simulations were run, using the WG and the customized Pyrex dishes, to find the distance from the short circuit, which allowed acceptable values of efficiency and CV at 1800, 1950, and 2450 MHz simultaneously. The distance of 140 mm from the short circuit was found to be the most suitable one, with the CV being around 35% in all the considered scenarios, while the efficiency

ranged from 30% to 40%. Efficiency and electric field uniformity were evaluated by means of power and calorimetric measurements, respectively, and were reported in [8] and summarized in Table 10 of D4.2.
As mentioned above, specific numerical and experimental dosimetry were carried out to improve the set-up described in the initial report to optimize the homogeneity of SAR distribution in the exposed samples. Numerical dosimetry analysis was carried out to expose four cell cultures simultaneously to two SAR values under homogenous field distribution. Specifically, parametric simulations were run to identify the distance of the samples' centre to the short-circuit that maximizes the efficiency and uniformity of electric field (and SAR) distribution in the four samples at both frequencies. The CST Microwave Studio 2024 (Dassault Systèmes Simulia, Paris, France) platform was used for simulations. The average SAR over the sample per unit of incident power (Watt per kilogram/Watt), was calculated as an indicator of the average specific efficiency. The Coefficient of Variation (CV), defined as the standard deviation of the SAR over the mean value, was adopted as an indicator of the SAR non-uniformity degree. Since the SH-SY5Y cell model grows adherent to the bottom of the dish, both parameters were calculated for the Whole Sample (WS) and for the Bottom Layer (BL). The overall efficiency (absorbed-to-incident power ratio) was also reported.

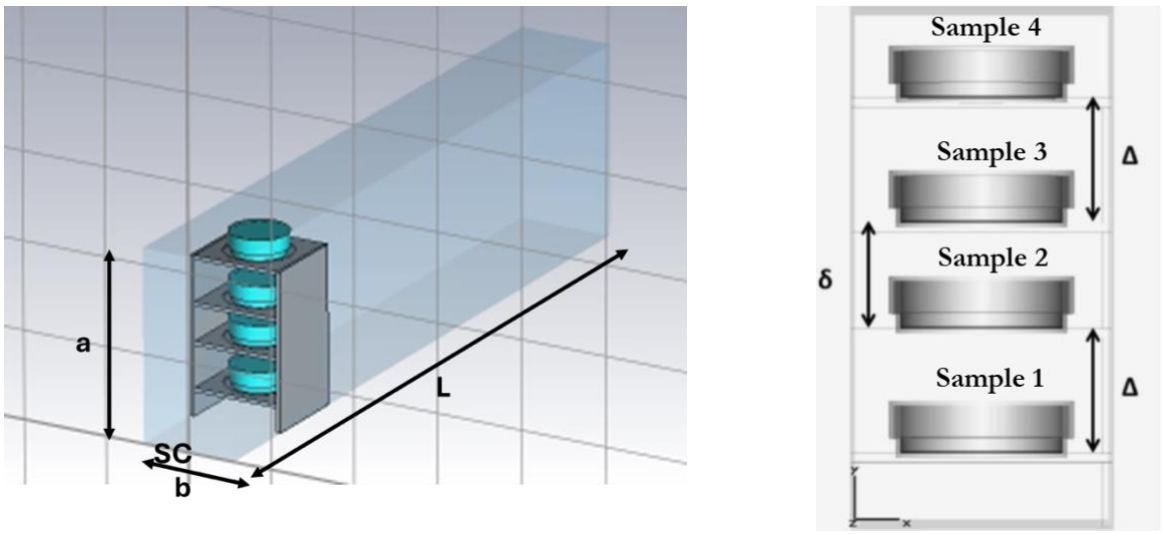

(a) (b)

Figure 15: Panel A: Geometric model of the waveguide (a = 109.2 mm; b= 54.6 mm; L= 350 mm) and of the four samples in 30 mm Pyrex dishes on the Plexiglas stand. SC: Short Circuit at 73.6 mm from the samples' centres. Panel B: detailed view of the four samples on the Plexiglas stand. The relative distances between the samples (δ = 22 mm; Δ = 26 mm) are set in such a way to obtain a 1:4 SAR ratio between the distal (sample 1 and sample 4) and the central (sample 2 and sample 3) positions of the stand.

The rectangular waveguide (inner transversal dimensions: 109.2 mm × 54.6 mm) was modelled as perfectly conductive with the longitudinal axis and narrow side horizontal, to achieve the condition of an unperturbed (empty waveguide) E vector parallel to the sample layer (Figure 15a). The four samples were modelled as DMEM cylinders (30 mm diameter, 3 mm thickness) placed inside four 30 mm, Pyrex dishes and located on a four-layer Plexiglas stand (Figure 15b). Electromagnetic properties of materials are reported in Table 11, while the mass density of DMEM samples was set at 1060 kg/m^3.

Table 11: Electromagnetic properties of materials set for numerical simulations.

	Pyrex		Plexiglas		DMEM	
	ε_r	σ [S/m]	ε_r	σ [S/m]	ε_r	σ [S/m]
1950 MHz	4.7	0	2.6	0	70	2.45
2450 MHz	4.7	0	2.6	0	70	2.9

The set-up for experimental dosimetry was the same as the one described in section 2.3.2.2. Power measurements were used to calculate the absorbed power as difference between incident and reflected powers (neglecting the waveguide power losses), and consequently to derive the average SAR as absorbed power divided by the overall mass. In order to exclude heating of the sample under the selected exposure conditions, temperature measurements were performed by using a FISO UMI4 (Quebec, Canada) thermometer with a fiber optic probe (FISO Technologies).

From the simulations, the distance between the samples' centers and the short circuit that maximizes efficiency and uniformity of SAR, resulted to be 73.6 mm. Table 12 shows the average SAR at 1 W incident power and CV, for each sample (both whole sample and bottom layer) at 1950 and 2450 MHz. The CV is around the desired value of 0.3 at 1950 MHz, and slightly higher (0.34-0.36), but still acceptable, at 2450 MHz [8]. Compared to the results described in section 2.3.3.2 of D4.2, where only one sample was considered for simultaneous exposures to multiple frequencies, the homogeneity of SAR distribution was improved in the current, four-sample configuration. Figure 16 reports the plots of SAR distribution in the BL, and the histograms of the SAR normalized to the average value for each sample exposed to 1950 and 2450 MHz.

Table 12. Average SAR at 1 W incident power and Coefficient of Variation (CV) for each sample (Whole Sample, WS, and Bottom Layer, BL) at 1950 and 2450 MHz.

[MHz]		Average SAR [W/kg/W]				CV			
		Sample 1	**Sample 2**	**Sample 3**	**Sample 4**	**Sample 1**	**Sample 2**	**Sample 3**	**Sample 4**
1950	**WS**	28.4	112.6	113.4	28.3	0.31	0.31	0.31	0.31
	BL	24.1	101.5	106.1	27.8	0.33	0.31	0.30	0.29
2450	**WS**	42	153.5	154.1	41.6	0.35	0.36	0.36	0.36
	BL	37.6	136.8	140.1	37.7	0.34	0.34	0.34	0.34

1950 MHz

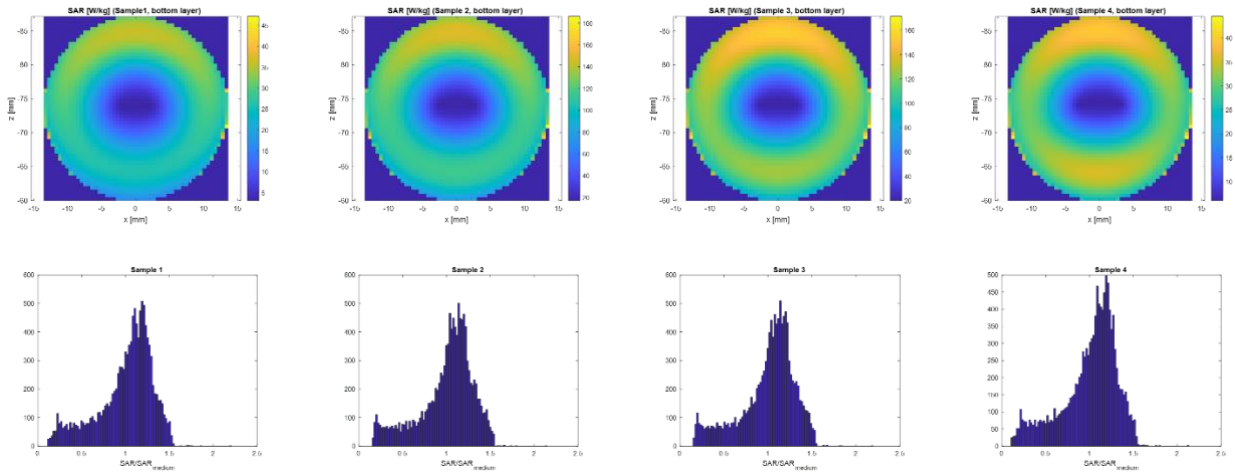

2450 MHz

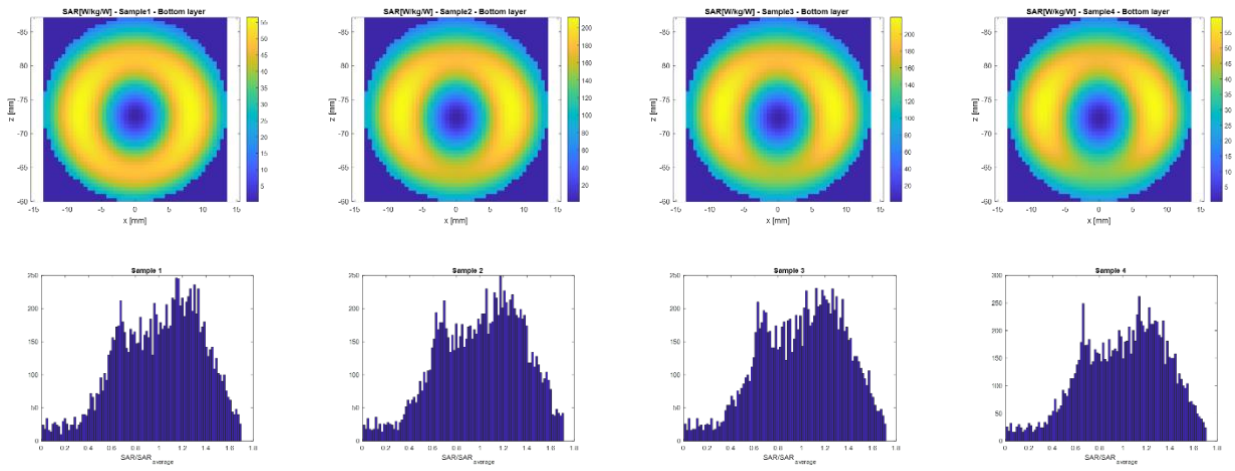

Figure 16: SAR distribution in the bottom layer of each sample, and histograms of the whole sample SAR normalized to the average value, obtained at 1950 and 2450 MHz.

Table 13. Comparison between average SAR and overall efficiency obtained by simulations and by power measurements. SAR_c and SAR_d are the SAR levels in the central and distal positions of the stand, respectively.

Frequency	Simulations			Power measurements		
	SAR_c [W/kg/W]	**SAR_d [W/kg/W]**	**Efficiency**	**SAR_c [W/kg/W]**	**SAR_d [W/kg/W]**	**Efficiency**
1950 MHz	113.4	28.3	52%	136.7±3.1	34.2	60%
2450 MHz	154.1	41.6	69%	165.5±0.25	44.7	72%

Table 13 shows the results of power measurements compared to those gained by numerical simulations. The measured average SAR_c and SAR_d and the overall efficiency were in satisfying agreement with the results of numerical simulations.

To verify the average levels and stability of SAR and temperature throughout the exposure period, the waveguide was loaded with the four samples in the Pyrex dishes and exposed for 3h at 1.25 W/kg average SAR in the central positions and 0.3 W/kg average SAR in the distal positions, that are the conditions foreseen for the biological investigations. The temperature measurement was performed by inserting the fiber optic probe in sample 3 (Figure 15b), which is one of the two central samples exposed to the highest average SAR value. Figure 16 presents the results of power and temperature measurements carried out simultaneously during RF exposure. The time-averaged SAR was 1.245 ± 0.024 W/kg (Figure 17a), whereas the temperature of the sample resulted stable at 35.66±0.03 °C during the 3h exposure (Figure 17b).

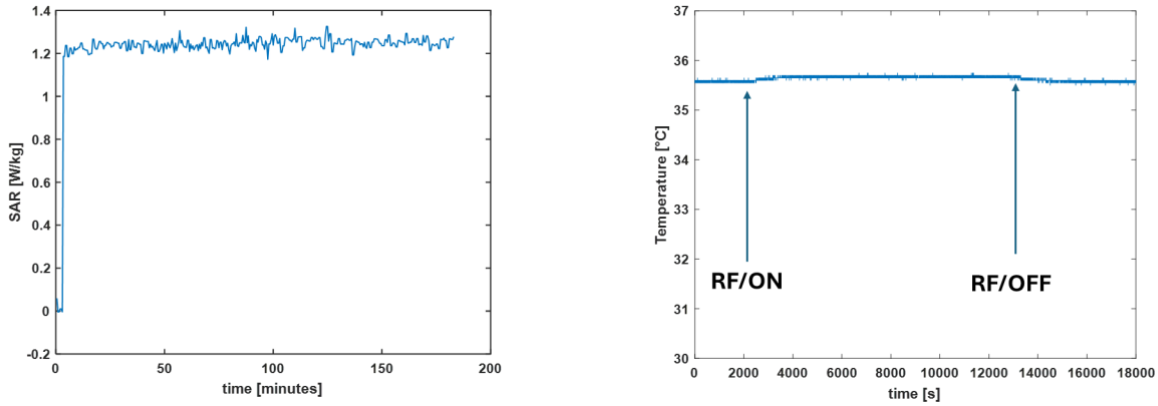

(a) (b)

Figure 17. Average SAR (Panel A) and temperature (Panel B) in sample 3 exposed simultaneously to 1950 and 2450 MHz for 3h.

3 Exposure systems in mm-Wave band

This Section is devoted to the presentation of the exposure systems to be used in the millimetre-wave band, that is in the FR2 band of 5G. As mentioned in the previous Section, due to the smaller wavelength different approaches have to be adopted with respect to the lower frequency band, since the exposed samples become comparable to the wavelength.

3.1 Exposure system at Sciensano

3.1.1 Introduction

The exposure system is intended to investigate the potential effects of a 5G signal on RBCs in humans.

This is a pilot study that aims to explore the potential effects of a short acute exposure to a 5G signal in the FR2 band in humans on the blood count and RBCs. Healthy volunteers (15 men and 15 women aged between 18 and 25) will be invited to take part in two double-blind, 45-minute sessions, one with real exposure and the other with sham exposure, in a randomized design. The exposure will be localized on the palmar surface of the forearm, at wrist level, which is preferred because of the proximity of blood vessels. A blood sample will be taken directly before and after exposure and analyzed. Additional information is available in D4.6.

Figure 18: Prototype of the box in which volunteers will place his/her uncovered forearm; the emitting antenna is located below, at the level of the wrist.

3.1.2 Setup description

The system is configured to generate a modulated 5G signal in the FR2 band according to the specifications defined in NextGEM (see section 3.2.2 of D4.1 for the specifications of the unified signal at the FR2 band). The generation/up-conversion system which will be used in the FR2 exposure experiments will be composed of the following sub/blocks units:

- **Signal generation with standard compliant stimuli:** The 5G signal will be implemented based on the numerology selected in Task 4.1 and the various (signal) frame parameters will be realized to maintain consistencies among the various experiments. The modulated signal is realized using a software-defined radio (SDR) unit or employing a vector signal generator in a frequency below 6 GHz as Intermediate Frequency (IF).
- **Signal up conversion:** the IF signal is moved to the FR2 band (i.e., 26.5 GHz) using a single side band (SSB) up conversion, and filtering stage.
- **Signal amplification:** the upconverted signal will be amplified using a linear amplification stage to allow reaching up to 20dBm at the coaxial port. Lower levels are achieved by using reduced drive levels at the mixer IF port.
- **Antenna selection:** the signal is then fed via an electronic controllable switch to one of the two exposure antennas in the setup.

The level at the conducted (coaxial) port will be defined with a lab calibration of the unit and a Look Up Table (LUT) will be generated to allow various power levels. The selected exposure level defined by the dosimetry analysis will then be used to select the required power level at the coaxial port from the LUT.

The proper functioning of the exposure system will be tested before each session. The volunteers will be seated in a comfortable armchair. On either side of the armrests, boxes will be placed where they will place their forearms (Figure 18); both boxes will contain an antenna placed below the inner face of the forearm: it will transmit the signals towards the palmar surface of the wrist (real or sham). The side selection is carried out in a double-blind fashion to avoid any bias affecting data evaluation. An area of about 20 cm^2 of the wrist will be perpendicularly exposed. Volunteers will be asked to hold a wooden strip in their palm so that the forearm and wrist are positioned correctly downwards during the exposure period.

The box is made of 1.9 cm thick wood. The positioning of the exposure system and the thickness of the box ensure that other parts of the body are excluded from exposure.

The test will take place in a 12-metre-long container (Figure 19, left) that is divided into two parts, one of them is the test room housing the volunteers and the experimenter for conducting the tests, together with the control equipment and the apparatus for measuring RF exposure levels. The other part is not used in this experiment. The test room is specially equipped with a comfortable chair, a table, and a chair (Figure 19, right). It is a setup to reduce the levels of environmental EMF (from the building and outside): the levels are < 0.1 V/m for RF EMF and < 0.05 μT for the 50 Hz magnetic field. When the exposure system is activated, exposure level is set to comply with the ICNIRP guidelines and the reference levels of Recommendation 1999/519/EC.

Additional details on exposure conditions are available in D4.6.

Figure 19: Left: container hosting both the technical room and the test room. Right: the interior of the test room.

3.1.3 Numerical dosimetry

Numerical dosimetry has been carried out by UCAS by means of CST Microwave Studio. Due to the frequency range involved, the Incident Power Density (IPD, see also D5.3) has been selected as target dosimetric quantity. The uniformity of the IPD was evaluated in terms of CV. Simulations were also useful to optimize the exposure system with respect to some design parameters, as detailed in the following.

The horn antenna and the wooden box have been modelled in CST and are shown in Figure 20. A transverse cut view of the overall system is shown in Figure 21. Since the IPD is, by definition, the power density distribution *in absence* of the target, the exposed forearm was not modeled.

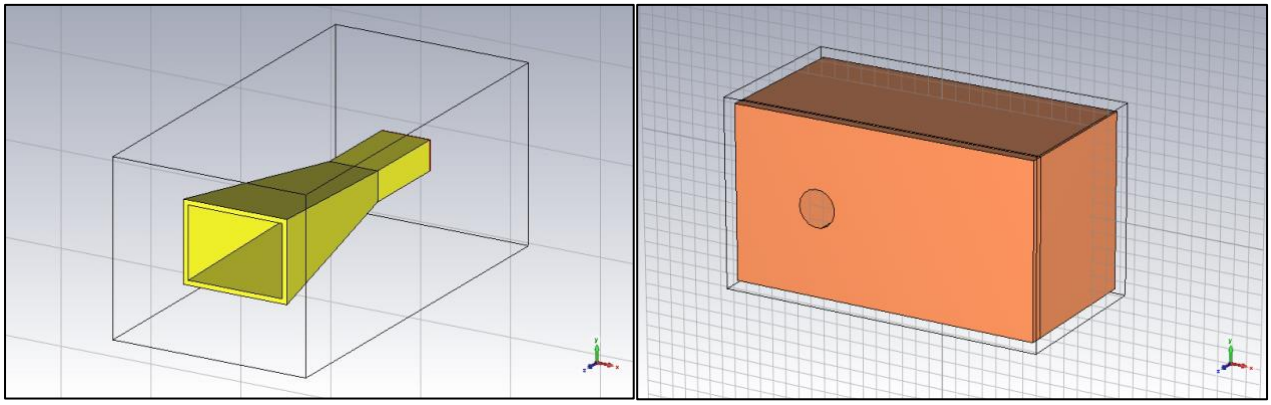

Figure 20: Horn antenna (left) and wooden box (right) modelled in CST.

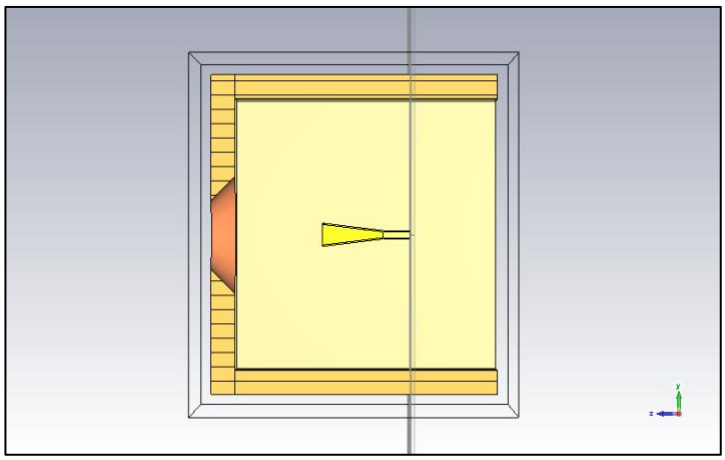

Figure 21: Cut view of the overall model in CST.

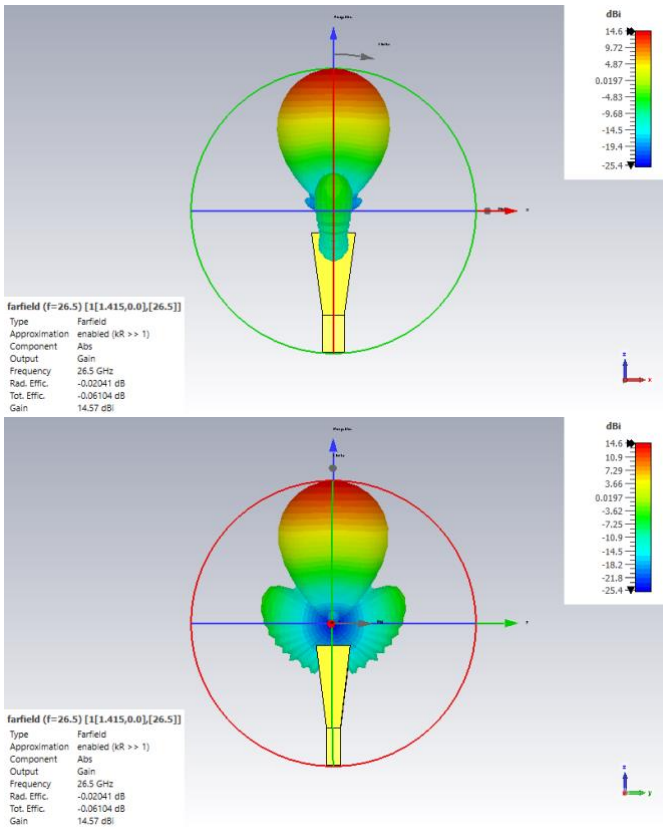

Figure 22: Radiation patterns of the horn antenna in the two principal planes.

The field radiated by the antenna exhibits an almost circular beam in the far field (see Figure 22 reporting the radiation patterns in the two reference planes), consequently a circular shape was selected. As a matter of fact, working in the far field region of the antenna was another assumption made since the beginning, also related to the selection of IPD as dosimetric quantity. As an example, a typical field distribution on the top of the box and on the aperture is shown in Figure 23.

In order to avoid any unwanted exposure and interference, the interior of the wooden box has been coated with the absorbing material ECCOSORB LS-22[4] with a thickness of 6.35mm. The wood of the box was characterized by the Microwave Lab at UCAS, to give a complex permittivity $\varepsilon_r = 1.71 - j0.10$. A thorough simulation campaign has been then carried out in order to optimize the edge cuts of the aperture in terms of CV, allowing to reduce the CV from about 50% in case of straight cuts, to about 20% in the case depicted in Figure 21, representing the best compromise taking into account both CV reduction and ease of manufacturing.

As a final result of the numerical dosimetry, the average IPD and the CV on the aperture are plotted in Figure 24 as a function of the distance of the antenna from the top of the box, for a reference input power of 1W. As can been seen, the CV is less than 22%, which is well below the 30% threshold commonly accepted in the literature. The average IPD curve represents a design curve allowing the selection of the proper configuration depending on the selected exposure level.

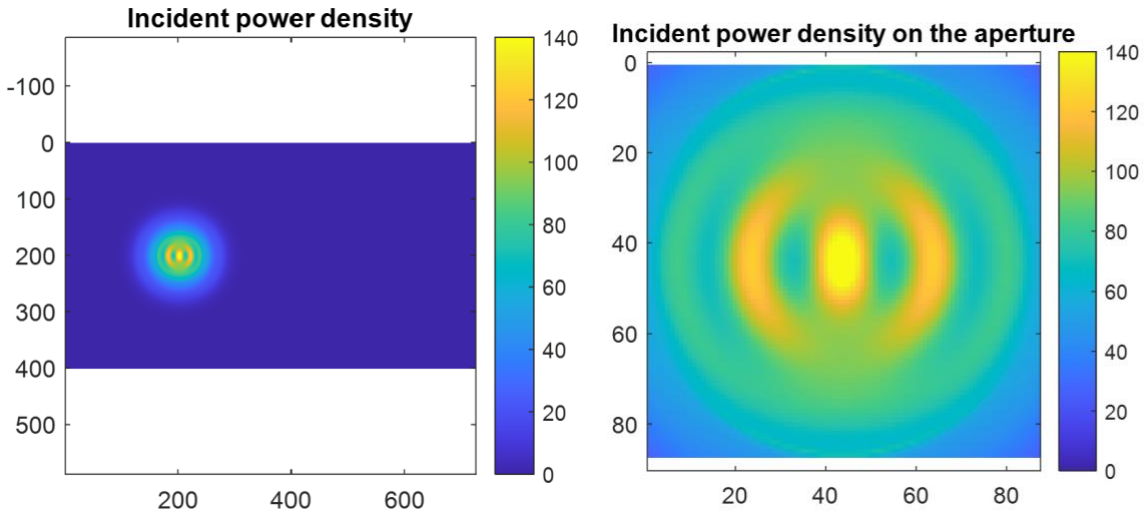

Figure 23: IPD distribution: on the top panel (left) and a zoom on the aperture (right).

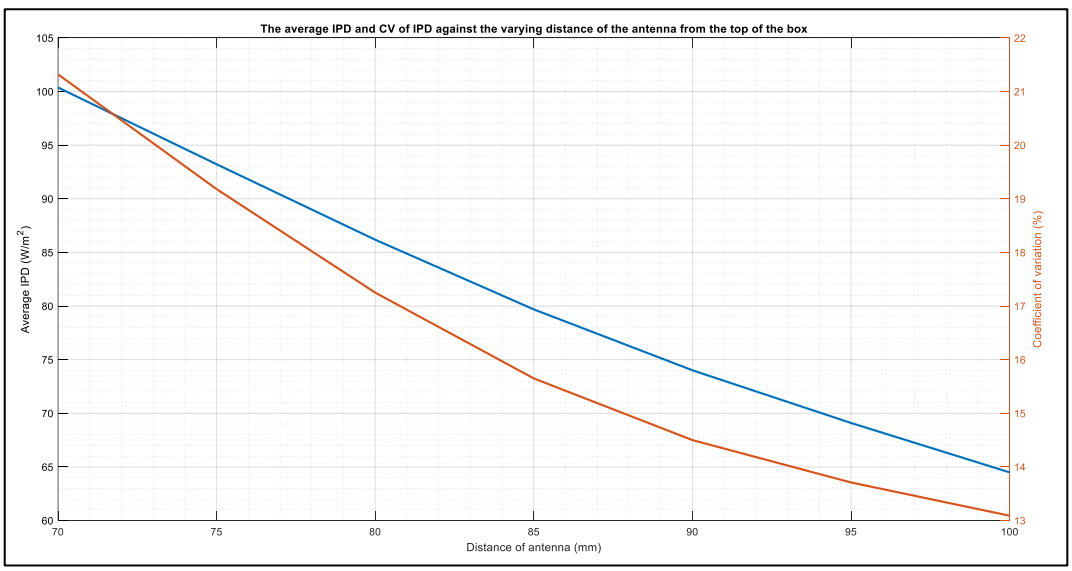

Figure 24: Average IPD and coefficient of variation (CV) as a function of the distance of the antenna from the top of the box. The input reference power is 1W and the frequency is 26.5 GHz.

[4] https://www.laird.com/products/absorbers/microwave-absorbing-foams/single-layer-foams/eccosorb-ls

3.2 Exposure system at CNR

3.2.1 Introduction

The Reverberation Chamber (RC) exposure system is used by CNR within the task 4.3 to expose HaCaT cells and *Caenorhabditis elegans* (*C. elegans*) nematodes at the frequency of 26.5 GHz (5G signal) by setting different SAR levels and exposure durations. In particular, HaCaT cells are exposed/sham exposed in the absence and in the presence of UVB radiation to analyse cancer-related endpoints such as oxidative stress, cell proliferation and apoptosis by applying flow cytometric techniques. Moreover, transcriptomic analysis (TempO-Seq) are also carried out on RF-exposed samples that are compared to the one carried out in SC on HaCaT cells exposed under the same conditions but at 3.5 GHz (5G signal). *C. elegans* nematodes are exposed/sham exposed to 5G EMF to evaluate oxidative stress (fluorescence microscopy, colorimetric assay) and changes in gene expression (RNAseq). Moreover, survival, reproduction and developmental rates are also evaluated.

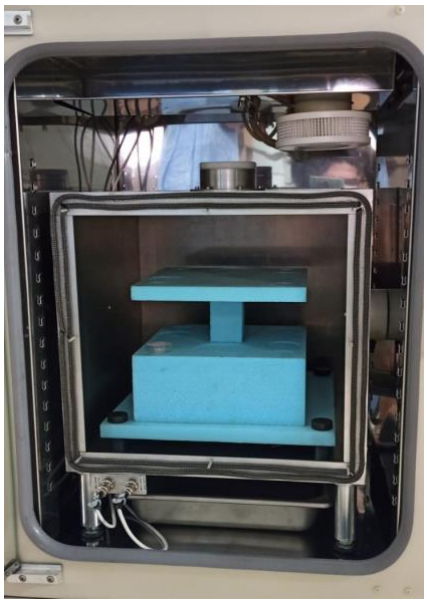

Figure 25: The reverberation chamber located inside the incubator.

3.2.2 Setup description

This exposure system has been designed, manufactured and characterized by UCAS (Figure 25). A RC is basically a resonator with very large dimensions compared to the wavelength so that a large number of modes can be excited. By cyclically changing the boundary conditions (through mechanical or frequency stirring), the modes configuration inside the chamber changes continuously, and the components of the resulting field have zero mean. The power density inside the chamber, on the other hand, is spatially uniform. As mentioned, a well-stirred RC must be electrically large to guarantee an effective stirring of the modes. For a rectangular shape, the mode density is given by the well-known formula [10]:

$$\frac{dN}{df} = \frac{8\pi abd}{c^3} f^2 - \frac{a+b+d}{c} \tag{10}$$

where c is the speed of light in a vacuum, f is the operating frequency and a, b and d are the dimensions of the chamber. Consequently, the dimensions of the proposed RC were chosen in order to have the largest available volume inside the incubator: the interior of the RC is 404 mm wide, 419 mm deep, and 375 mm high and the wall thickness is 4 mm. The resulting theoretical mode density is 43 modes/MHz at 27 GHz.

The stirrers are two rectangular metallic crosses (each arm being 22mm large and 300mm long) rotating parallel to two perpendicular walls (on the bottom and on the wall opposite to the feeding port) at independently controlled velocities. The RC is realized in anticorodal (aluminium-magnesium-silicon alloy) that exhibits a good electrical conductivity ($3.57 \cdot 10^7$ S/m), weldability, resistance to corrosion and it is easy to handle. An opening (8cm diameter) with a metal net (mesh: 200μm) was inserted in the top wall to guarantee constant environment (temperature, relative humidity, and CO_2) when the RC is inserted into the incubator. A stand with housings for Petri dishes opportunely engraved allows a reproducible positioning of Petri dishes. Two WR-28 open-ended waveguides are used as transmitting and receiving antennas. The RC is located inside the incubator and is connected to a signal generator SMW200A by Rohde&Schwarz with SMW-K144 and SMW-K148 options enabled

to generate a 5G compliant signal. The delivered power is measured during the exposure by means of a power meter (Rohde&Schwarz, NRP-Z85) connected to the feeding line through a directional coupler (Marki Microwave, CA40).

3.2.3 Numerical dosimetry

The RC is a microwave two-ports system which can be characterized by its scattering parameters (s-parameters). In an ideally performing RC (which implies that the chamber is well stirred with a large number of modes and a large mode-density), the S-parameters have zero mean. On the other hand, due to the unavoidable mismatch of the feeding antennas and to the direct path between antennas, the measured parameters do not satisfy the zero-mean condition. Given the measured parameters S'_{ij}, the S-parameters related to the stirred contribution only, can be calculated as [11]:

$$S_{ij} = \frac{S'_{ij} - \langle S'_{ij} \rangle}{\sqrt{1 - \left|\langle S'_{ii} \rangle\right|^2}\sqrt{1 - \left|\langle S'_{jj} \rangle\right|^2}} \tag{11}$$

where the unstirred contribution has been removed and the antenna mismatch has been corrected. Once the parameters defined by (11) are calculated, the RC is fully characterized, and all the relevant related quantities can be calculated, such as the enhanced backscatter coefficient and the Quality factor (Q), representing the main quality figures of the system.

The enhanced backscatter coefficient has been evaluated as [11]:

$$e_b = \frac{\sqrt{\langle |S_{11}|^2 \rangle \langle |S_{22}|^2 \rangle}}{\langle |S_{12}|^2 \rangle} \tag{12}$$

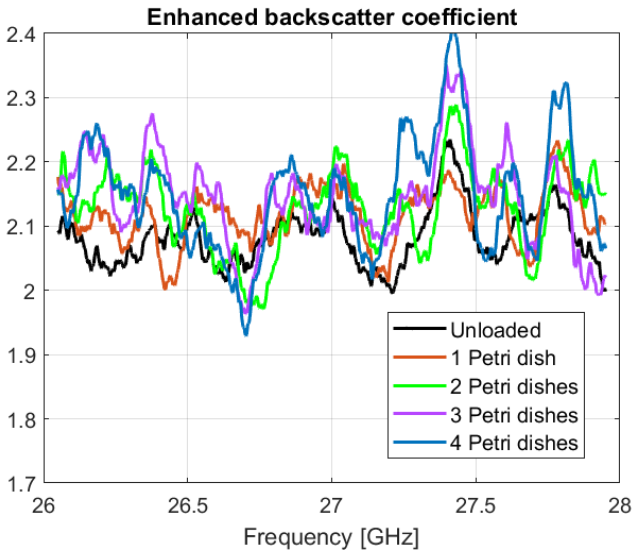

Figure 26: Enhanced backscatter coefficient for different loading conditions of the RC.

In an ideal RC $e_b = 2$, so the deviation from this value represents a quality figure of the chamber performance. In Figure 26 e_b is plotted both in the unloaded case, and with up to 4 Petri dishes. As can be seen, it is very close to the ideal value when the RC is unloaded, with a deviation of about 5% in most of the frequency range. Of course, when the scatterers are inserted, the deviation is slightly larger, but anyway limited.

The Quality Factor is another parameter describing the performance of the RC, as well as of any resonant system. It is related to the parameters of the RC by the well-known relationship:

$$Q = \frac{\omega W_{em}}{P_d} = \frac{V\frac{16\pi}{\lambda^3}\langle |S_{12}|^2 \rangle}{1 - \langle |S_{11}|^2 \rangle - \langle |S_{12}|^2 \rangle} \tag{13}$$

where ω is the angular frequency, W_{em} and P_d are the stored electromagnetic energy and dissipated power in volume V respectively, and λ is the wavelength. According to (13), the Quality Factor has been measured with different loading conditions and is plotted in Figure 27. The order of magnitude of the quality factor is in very

good agreement with that estimated, for example, in [12], and anyway much larger than the threshold metric introduced in [13] as:

$$Q_{thrp} = \left(\frac{4\pi}{3}\right)^{\frac{2}{3}} \frac{3V^{\frac{1}{3}}}{2\lambda} \cong 140 \tag{14}$$

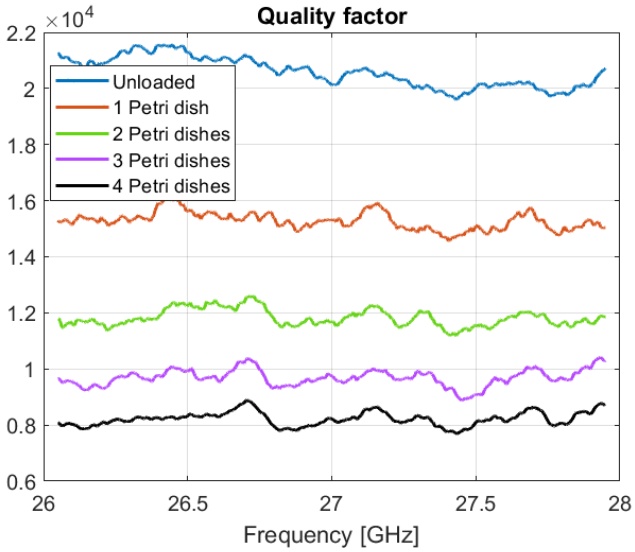

Figure 27: Quality Factor for different loading conditions of the RC.

Once the performance of the RC has been demonstrated to be in very good agreement with that of an ideal chamber, the theory developed by Hill [10] can be applied in order to simplify the numerical dosimetry. As a matter of fact, since the RC is, by design, very large with respect to the wavelength, a direct simulation of the Petri dishes in such a huge volume would require a huge amount of resources. On the other hand, Hill demonstrated that the field distribution in the RC can be evaluated by resorting to the classical plane waves integral representation: the statistics of electric and magnetic fields can then be determined in terms of probability density functions and spatial correlation functions. In particular, the mean value of the electric field is zero, whereas the mean-square value of the electric field is independent of position. With reference to the probability density functions, it can be shown that the electric field components are Gaussian, whilst their absolute value has a Rayleigh distribution. The uniformity of the field is a key-point in the context of exposure systems designed for biological experiments, which makes RCs very appealing. On the other hand, when resorting to numerical dosimetry, the number of plane waves to be taken into consideration is obviously finite, and a compromise has to be found between accuracy and calculation times. A discussion on the number of plane waves to be considered and the validation of the model by means of regularized semi-analytical techniques, can be found in [14].

According to the discussion above, the numerical dosimetry has been carried out by means of CST Microwave Studio, simulating a suitable number of plane waves impinging on one (or more) Petri dish and superposing the computed fields. The waves have unitary amplitude and both polarizations have been considered; the incoming directions have been uniformly distributed in azimuth and elevation. The statistics of the SAR have then been evaluated and the SAR degree of uniformity estimated by means of CV. The mesh used in the simulations was as fine as 0.010 mm in the lower 100 μm of DMEM, corresponding to the cell monolayer, and 0.1mm in the higher part of DMEM.

An example of the SAR distribution when a single wave is impinging, and when 12 waves are considered is plotted in Figure 28. The smoothing effect of the superposition of waves is apparent, limiting the non-uniformity to the unavoidable edge effects. The z-axis is taken along the Petri axis, the origin being at the bottom of the culture medium, so the monolayer under investigation lies in the [0μm, 100μm] range. An example of the SAR distribution at z = 20 um when 12 plane waves are impinging on 4 Petri dishes is shown in Figure 29. It is worth noting that in the real system the waves superposed are many more than twelve, so even this case is overcome in practice. For instance, in Table 14, the CV is reported for different slices of the monolayer when considering 12 and 28 waves impinging on the Petri dish.

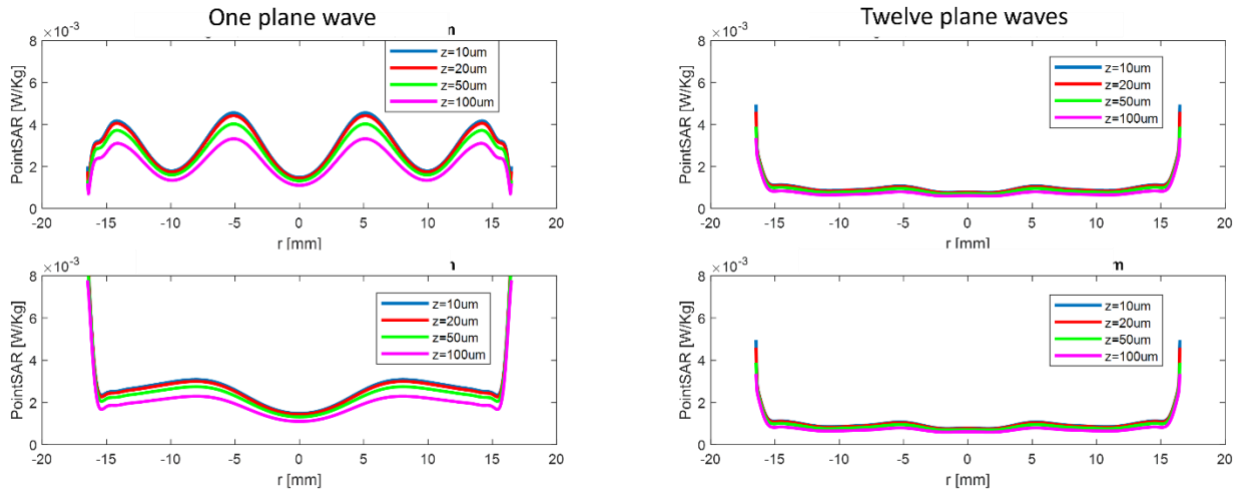

Figure 28: An example of the SAR distribution at different quotes when a single plane wave is impinging on the Petri dish (left) and when 12 plane waves are considered (right).

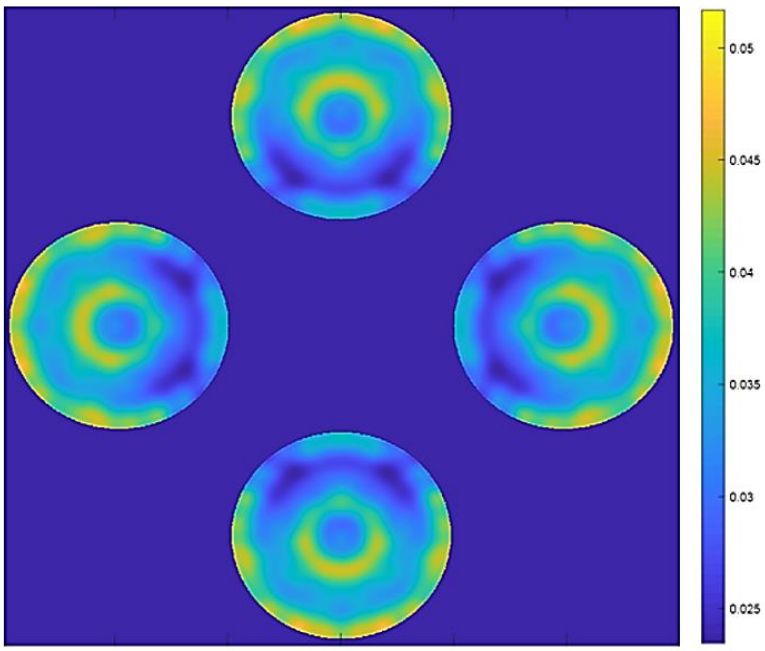

Figure 29: An example of the SAR distribution at 20 um in 4 Petri dishes with 12 impinging plane waves. The Petri dishes are spaced apart 50 mm in the horizontal and vertical directions.

Table 14: CV in different slices of the monolayer when considering 12 and 28 waves.

z_{slice} [um]	12 waves	28 waves
	CV	**CV**
11	0.277	0.202
21	0.280	0.205
31	0.283	0.208
41	0.286	0.212
51	0.290	0.215
101	0.315	0.243

3.2.3.1 Temperature measurements

It is very important to keep the temperature of the exposure environment to about 36 °C in order not to induce stress in the exposed samples, which is one of the tasks performed by the incubator. On the other hand, the RC itself is a large metallic box inside the incubator, so measurements have been carried out in order to verify the thermal behaviour inside the RC. In Figure 30, the temperature trend inside the RC, measured by means of a fibre optic thermometer, is shown when no RF is on: the RC starting temperature is the environment temperature, and then it increases until it reaches 36 °C. It is worth noting that it takes about 4 hours to reach the target temperature. This is very important information, implying that some time (hours) is needed before inserting the samples and starting the exposure when the RC is put inside the incubator.

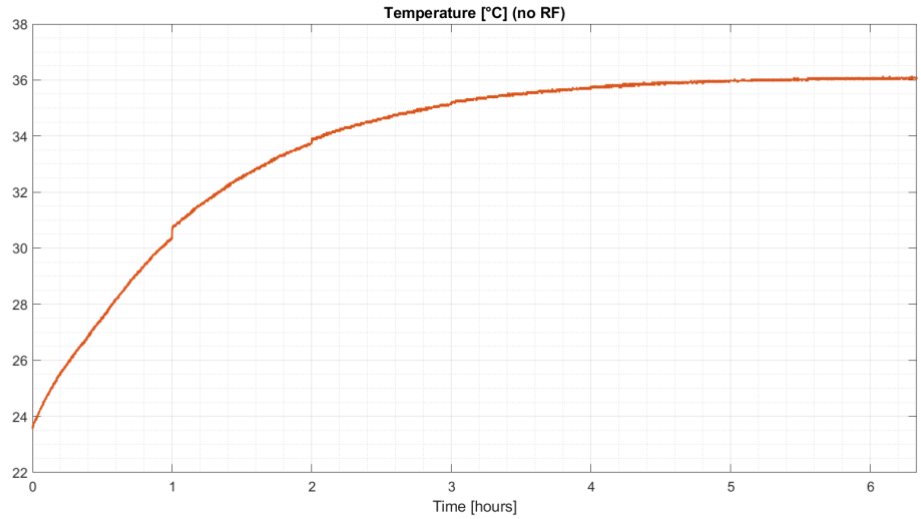

Figure 30: Temperature trend inside the RC without RF signal.

The temperature trend has been measured also when the RF is turned on, in order to check if any kind of temperature change was induced in the sample by the EMF. The result of this measure is plotted in Figure 31, where the RF is turned on after two hours. As can be seen, during the first two hours the same trend in the temperature increase can be observed as in Figure 30 (note that the time scale is different). Once the RF is turned on, anyway, the temperature change during the following 18 hours is within 0.1 degrees, which is within the thermometer tolerance.

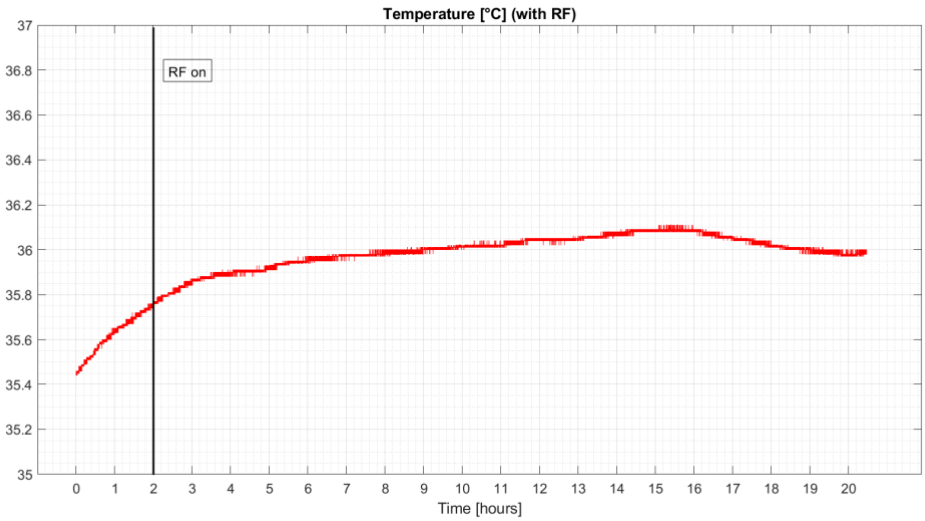

Figure 31: Temperature trend inside the RC with RF signal.

4 Exposure of heavy and light mobile users

In this part, we will attempt to consider human exposure in a real setting. For this part, biological effects in human buccal cells will be evaluated based on the usage behaviour of mobile phones. At the beginning of the study, 30 "light" mobile phone users and 30 "heavy" mobile phone users will be selected according to their self-reported usage behavior. However, previously it has been reported that self-reported data are often poor predictors of actual real usage [15]. Light users generally overestimate their usage, whereas heavy users tend to underestimate their mobile phone activity. To remedy this, we will make use of a mobile phone app (xMobisensePlus) to determine the level of exposure (and any related biological effects) in the volunteers, with their everyday use, without any specific outside exposure. Their level of exposure will be supplemented by an interview where they will be asked about their self-reported usage behaviour along with the recorded phone data, such as voice call (yes/no), MobileData (on/off), Wi-Fi connection, network type, network quality parameters (f.i. Received Signal Strength Indicator, Reference Signal Received Power, Reference Signal Received Quality, etc.), among other factors. These will then be used to determine a measure for downlink exposure. The volunteers will have the app installed on their phone during the first meeting after filling out the Informed Consent Form (ICF) and questionnaire. A buccal cell sample will also be taken for further analysis. This app will keep running on their phone for a predetermined amount of time (1 week), after which the data will be extracted from their phone, and a second buccal sample will be taken. While this approach is not perfect and does not take into account environmental exposure, it should provide a more reliable measure of determining exposure than self-reported data from their phones.

Upon selection of the volunteers, the participants will also have to fill out a questionnaire, which includes a wide range of questions, such as an estimation of time spent on the phone, as well as the model of the phone and the potential presence of jewellery in the ear or fingers, which can be relevant for the modelling of expected exposure values coming from the phone themselves, based on characteristics of the phone , which will be modelled by UCAS. For further information on this modelling, see 4.1. in this Deliverable.

The micronucleus assay will be applied to exfoliated buccal cells of heavy and light mobile phone users to determine genotoxicity. In addition, gene expression analysis will be conducted by utilizing RT-qPCR on genes of interest previously identified in the *in vitro* studies, to validate the *in vitro* results in a realistic exposure scenario and to see if the exposure to RF-EMF from mobile phones will be sufficient to elucidate a different expression in the genes that were previously found to be elevated as a result of mobile phone exposure. We take a sample at both timepoints to have a measure of biological variance in the same participant, assuming the behaviour, both in terms of phone usage and in terms of environmental factors has not changed drastically during the time of the experiment.

4.1 Numerical dosimetry

The numerical dosimetry related to task 4.4 is currently under development. Some preliminary simulations have been carried out in order to get acquainted with the simulation protocols and to gain some sensitivity on the models of humans. Some preliminary results are presented in the following.

CST Microwave Studio makes available many different models of humans, which differ with respect to the sex and age of the subjects and to the resolution of the models (see Deliverable D3.3 for a comprehensive description of the models available in the literature). For this preliminary analysis we selected two models: Hugo and Zubal. Both are whole-body models, but for our purposes, we focused only on the head. In particular Hugo is modelled with 31 different tissues and a voxel dimension of 1mm x 1mm x 1mm, whereas Zubal has 87 tissues but a voxel dimension of 3.6mm x 3.6mm x 3.6mm. The Samsung J5 mobile phone model, already available on CST Microwave Studio, was used for the simulations, but it was equipped with a suitably designed 5G antenna working at 3.6 GHz.

A particular attention was devoted to the position of the mobile phone with respect to the head. As a matter of fact, standard IEC/IEEE 62209-1528 [16] defines how to carry out simulations for exposure assessment by hand-held devices: two configurations are indicated, named "cheek" and "tilted" in the standard. In the following, the steps to correctly configure the two cases are reported.

a) Identify the reference axes (Figure 32):
- the B-M line connecting the reference points of the mouth (M) and the back of the head (B);
- the N-F line connecting the reference point of the forehead (F) to that of the neck (N);
- the Ear Reference Point (ERP) point which constitutes the reference for the ear and is distinct for the right (RE) and left (LE) side;

- the ERP is identified along the B-M line, 15 mm from the entrance of the ear canal. It is necessary to place these references externally to the phantom, as in the figure, to facilitate the positioning of the mobile phone.

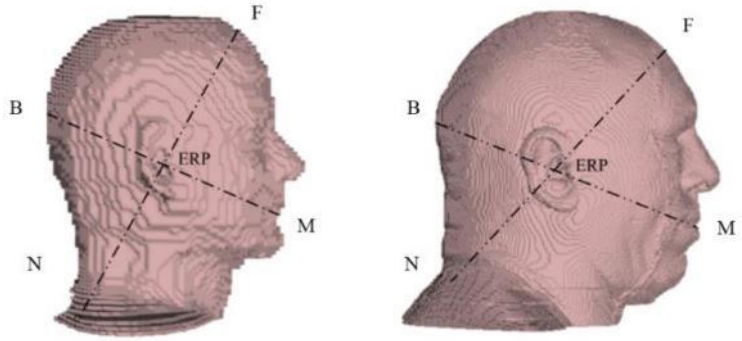

Figure 32: Reference points and lines of the Zubal (left) and Hugo (right) models.

b) For the Device Under Test (DUT) it is necessary to mark two reference lines on the front surface (Figure 33):
- the vertical centre line
- the horizontal line

The vertical central line passes in the upper part of the DUT at the point corresponding to the centre of the audio output and is indicated with the letter A, while in the lower part, it intersects the midpoint indicated by the letter B. Once this first reference has been identified, the second is obtained by tracing a line orthogonal to it and crossing it at A. Together, these two lines define a reference plane which must be parallel to the sagittal plane of the anatomical head.

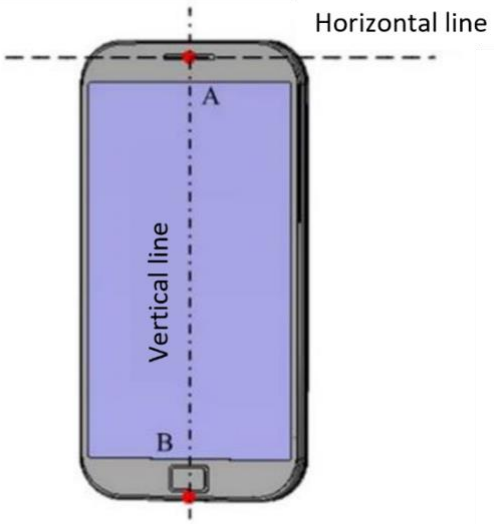

Figure 33: Reference points and lines for the DUT.

c) The origin of the reference system for the anatomical head model coincides with the ERP of the ear taken into consideration for the simulation and the right-handed triple, which constitute the axes defined as follows:
- the z-axis coincides with the virtual D-LE line and points towards the outside of the ear;
- the y-axis lies in the reference plane along the B-M line;
- the x-axis is perpendicular to the reference plane and cuts it at the ear's ERP. This axis is located along the NF-F line.

The origin of the reference system is placed at the centre of the mobile device screen.

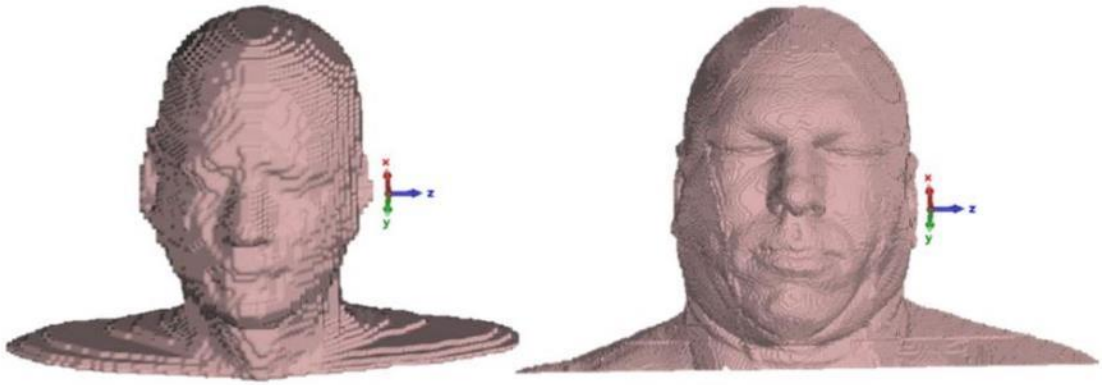

Figure 34: Coordinate system for the Zubal (left) and Hugo (right) model.

Once the identification procedure is completed, we proceed with the geometric transformations of translation and rotation of the DUT to arrange it according to the cheek position through the following steps:

a) move the mobile phone by sliding point A along the straight line that connects the two reference points RE and LE, until it comes into direct contact with the ear. The plane identified by the two reference lines of the telephone must be parallel to the sagittal plane of the human model;
b) rotate the mobile phone around the virtual line RE-LE until the central vertical line is in the reference plane identified by the NF-F and B-M lines;
c) maintaining contact of the DUT with the auricle, rotate the mobile phone around the N-F line until any point touches another point of the cheek;
d) rotate the mobile phone around the NF-F line passing through A until the ventral vertical line is in the reference plane.

The positioning in the "tilted" configuration requires three more steps after the "cheek" configuration has been obtained (Figure 36):

e) move the mobile phone away from the pavilion to allow it to rotate;
f) rotate the phone with respect to the line orthogonal to the virtual RE-LE line by an angle of 15°;
g) bring the device closer to the phantom until any part of it touches the ear.

After practising and mastering the above-mentioned procedure, some preliminary results have been calculated to check the consistency of the model. The maximum SAR, averaged over 10g, has been computed in the overall head and in some selected tissues. In Table 15, the computed values are reported with reference to salivary glands and the overall head for the two positions of the mobile phone. The results are perfectly consistent with the data provided by the mobile phone manufacturer.

Table 15: Computed values of maximum SAR averaged of 10g.

	Position	Maximum SAR [W / kg W]
Head	Cheek	1.65
	Tilted	1.07
Salivary glands	Cheek	0.0939
	Tilted	0.0445

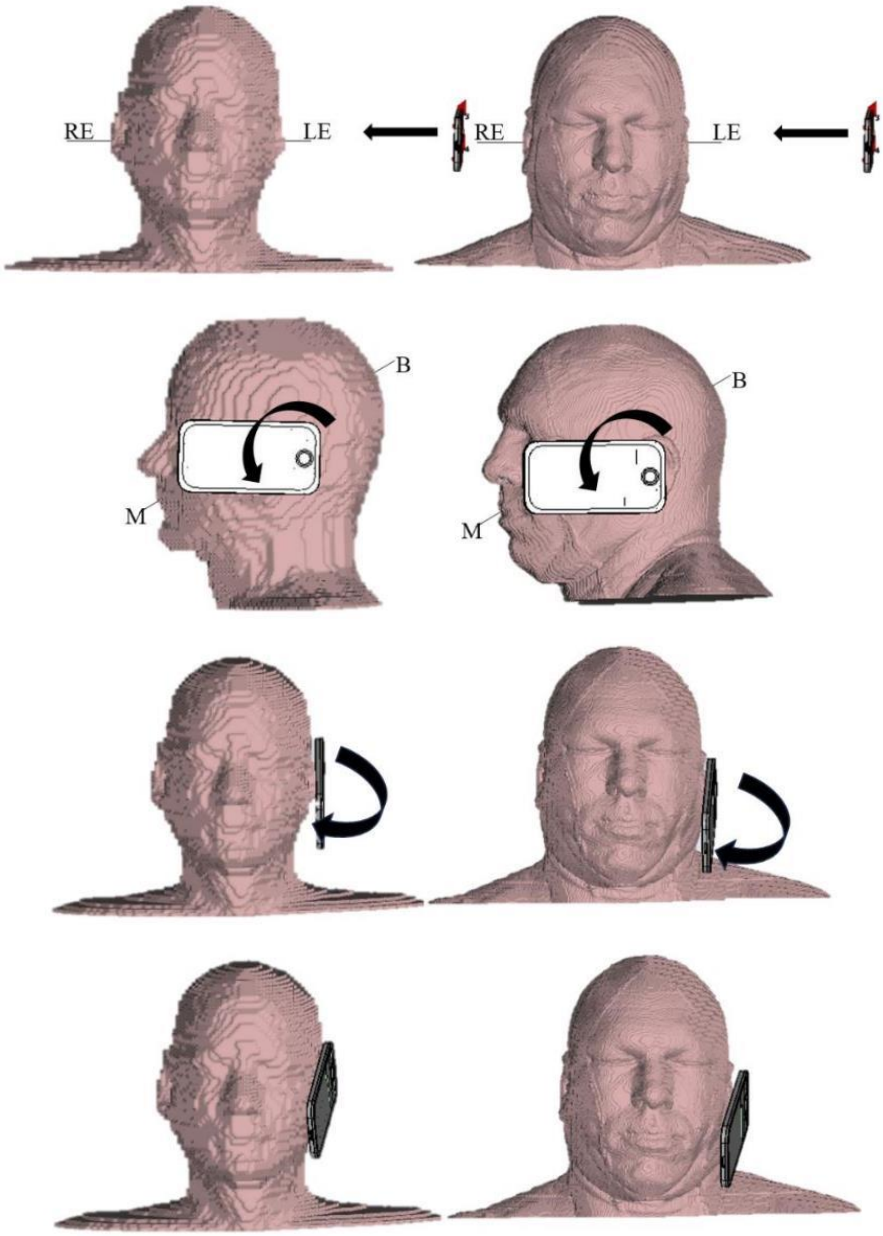

Figure 35: Sequence of steps of the positioning procedure for the left side.

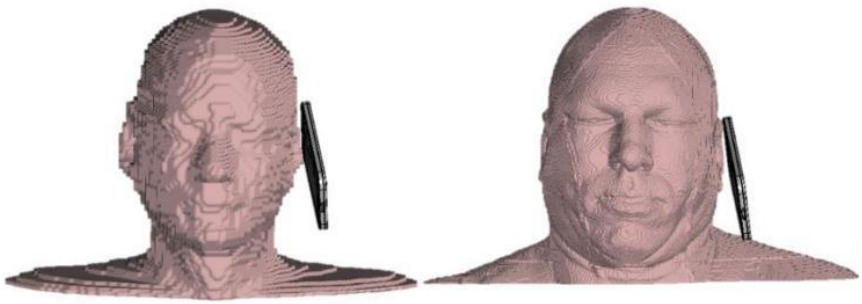

Figure 36: Final position in "tilted" mode.

5 Electromagnetic characterization of materials

The investigation of the interaction between EMF and biosystems relies on the knowledge of the electromagnetic characteristics of the materials involved in the experiments: these include, for example, the culture media for the cells. The electromagnetic characterization of materials is a widely studied problem, and there are several methods available in the literature [17][18]. Among them, the method using truncated coaxial cables as probes is particularly suitable for wideband permittivity characterization of solids and liquids [18]-[23]. These methods are based on the measurement of the reflection coefficient at the tip of a truncated coaxial cable placed in contact with the material under test (see Figure 37) and connected to a Vector Network Analyzer (VNA).

There are two key steps in this approach. The first one is the evaluation of the functional relationship between the reflection coefficient of the coaxial cable radiating toward a half-space and the electromagnetic characteristics of the material filling the half-space. The second one consists of developing a suitable calibration technique able to retrieve from the measurements at the gate of the VNA (section A in Figure 37) the reflection coefficient at the tip of the cable (section B in Figure 37).

All the proposed procedures implementing this method essentially differ in these two steps.

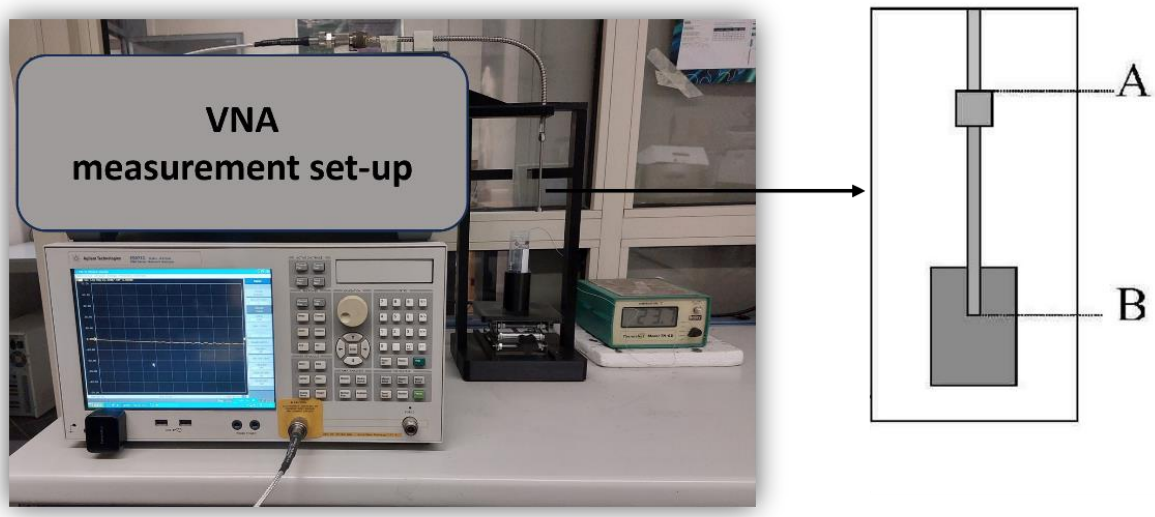

Figure 37: The permittivity measurement system. Left: truncated coaxial cable placed in contact with the Sample Under Test (SUT); right: sketch of the cable and reference plane where the reflection coefficient is evaluated.

5.1 Models

In our approach we use for the step one the expression of impedance of a truncated coaxial cable developed in [19], where a Rational Function Model (RFM) for the impedance of a standard 50 ohm semi-rigid coaxial cable (diameters 2.2 and 3.6 mm) is introduced allowing the permittivity evaluation in a quite simple way; moreover a satisfying accuracy is achieved in the case of lossy medium as expected in the case of biological samples [22]. The RFM developed by Stuchly et al. [24] and Anderson et al. [19] is a closed-form analytic model of the inverse problem used to determine the permittivity of a dielectric medium from the measured reflection coefficient of an open-ended coaxial probe. The model was derived assuming an idealized configuration of a 50- semirigid Teflon-filled coaxial line with an infinite flange radiating into an infinite homogeneous dielectric medium. It was determined to be valid in the 1–20 GHz frequency range (but it can be extended also to slightly higher frequencies) for $1 \leq \varepsilon_r' \leq 80$ and $0 \leq \varepsilon_r'' \leq 80$, where $\varepsilon_r = \varepsilon_r' - j\varepsilon_r''$ is the complex dielectric constant of the medium under test.

The relationship between ε_r and the aperture admittance Y^{model} is given by the following RFM:

$$Y^{model}(s, \varepsilon_r) \cong \frac{\sum_{n=1}^{N}\sum_{p=1}^{P} \alpha_{np}(\sqrt{\varepsilon_r})^p (sa)^n}{1 + \sum_{m=1}^{M}\sum_{q=1}^{Q} \beta_{np}(\sqrt{\varepsilon_r})^q (sa)^m} \tag{15}$$

where s is the complex frequency, a is the radius of the inner conductor of the coaxial line, and α_{np} and β_{np} are the model coefficients [24]. For a given measurement frequency and measured admittance, (15) becomes a polynomial in $\sqrt{\varepsilon_r}$. In all cases investigated, there is only a single physically meaningful root of the polynomial: the square root of the permittivity.

In order to reduce the uncertainty, measurements on one (or two) known liquid(s) are needed, as described in the following section. The liquids can be modelled by means of the Cole-Cole dispersion relationship:

$$\varepsilon = \varepsilon_\infty + \frac{\varepsilon_0 - \varepsilon_\infty}{1 + (j2\pi f\tau)^{1-\alpha}} \tag{16}$$

where f is the frequency, and ε_∞, ε_0, τ and α are the parameters to be determined during the inversion process.

5.2 Measurement techniques

Concerning the second step, we used the calibration technique proposed in [20] based on the characterization of the response of the coaxial probe using known loads. This method resembles the standard error correction techniques used in VNA and requires terminating the probe on three known loads, in our specific case, a short circuit (s), an open circuit (o) and a liquid (l). With reference to Figure 38, the three scattering coefficients S11, S12*S21, S22 [25] are obtained by inverting the three non-linear equations relating the measured reflection coefficients Γ_{ms}, Γ_{mo}, Γ_{ml} (wherein m stands for 'measured' value at section A of Figure 37) with the reflection coefficients at the tip of the probe, Γ_s, Γ_o, Γ_l (i.e. at the Section B of Figure 37) obtained by the rational function interpolation formula. The advantage of this approach is that it can correct, at least partially, errors that can affect the measurements as well as the unavoidable representation error of rational function interpolation formula or other selected impedance formulas of truncated cable [20].

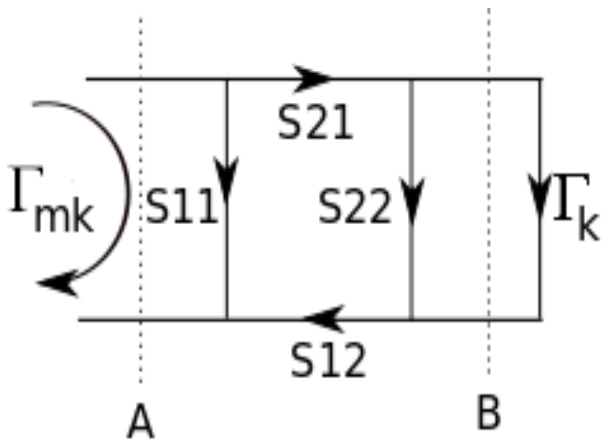

Figure 38: Probe calibration: flow-graph of the microwave signal; Γ_{mk} is the measured reflection coefficient (section A in Figure 37), Γ_k is the reflection coefficient at the tip of the probe (section B in Figure 37); k indicates the load used in the calibration process (k=o for open circuit, k=s for short circuit, k=l for known liquid).

5.3 Measurement results

By applying the technique described above, some measurements have been carried out at the Microwave Laboratory at the University of Cassino and Southern Lazio. A VNA R&S ZNA43 with calibration kit ZV-Z229 was used, together with a makeshift truncated coaxial cable (UT141, 3.6 mm external diameter). The DMEM was characterized since it is the culture medium of HaCaT cells. Moreover, the Nematode Growth Medium (NGM), to be used for *C. elegans* exposure has been characterized in the absence and in the presence of a high concentration of nematodes. The real part and the imaginary part of the measured permittivity are plotted in Figure 39 for the different media. As can be seen, the presence of nematodes has a minimum impact on the value of the permittivity.

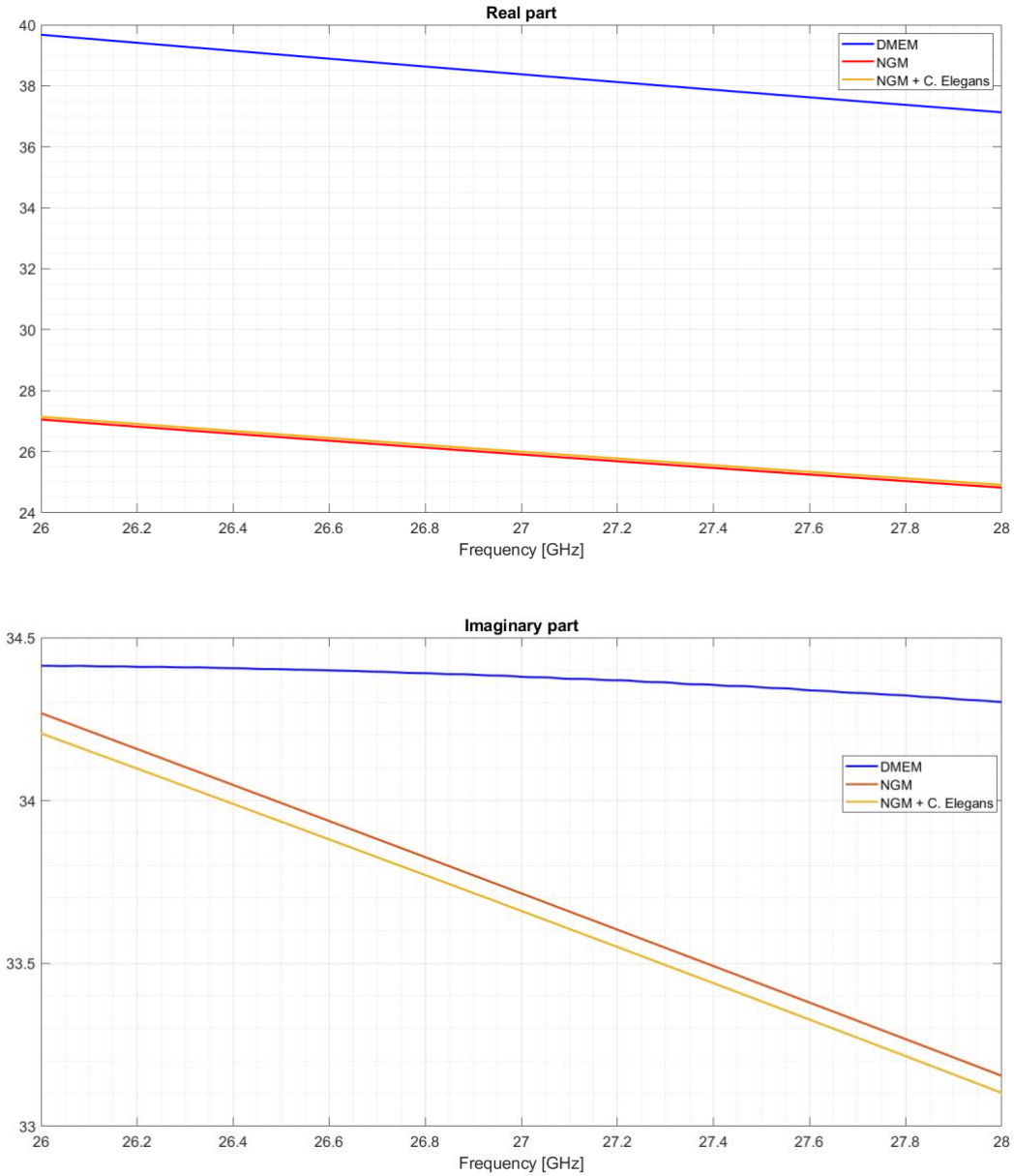

Figure 39: Real and imaginary part of the measured relative permittivity of DMEM (at 37 °C), NGM and NGM with *C. Elegans* (at 20°C).

5.4 Improved interferometric techniques

As discussed in previous sections, broadband dielectric measurements can be performed by means of an open-ended coaxial probe measurement. These measurements are constrained, from the point of view of the achievable sensitivity (i.e., minimum permittivity difference/variation distinguishable), from the complex noise behavior of VNAs used in these test benches.

VNAs can achieve low measurement noise and thus high sensitivity only when measuring devices under test (DUTs) with impedance levels close to the VNA instrument impedance (Z0), commonly designed to be 50 Ω, as can be seen in Figure 40.

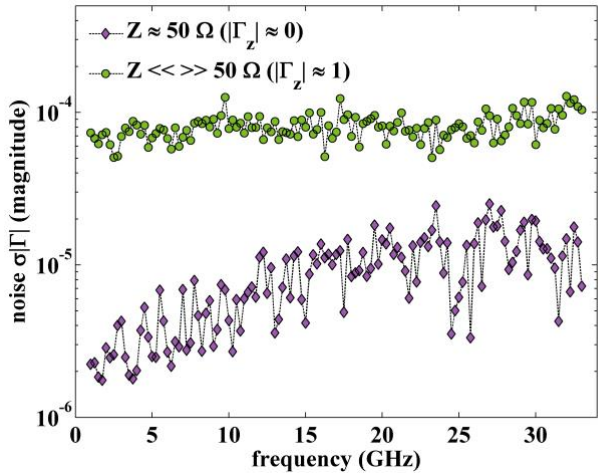

Figure 40: VNA input reflection coefficient (Γ) noise as a function of frequency for a high-reflection (Γ=1) and low-reflection (Γ=0) coefficient device

For this reason, various techniques have been presented in the literature to cancel the device generated b-wave by superimposing a second wave, with opposite phase, effectively realizing an electrical high frequency interferometer.

Here a technique, as described in [26], based on an IQ interferometer is employed, see Figure 41, in open-ended coaxial measurements to increase the system sensitivity.

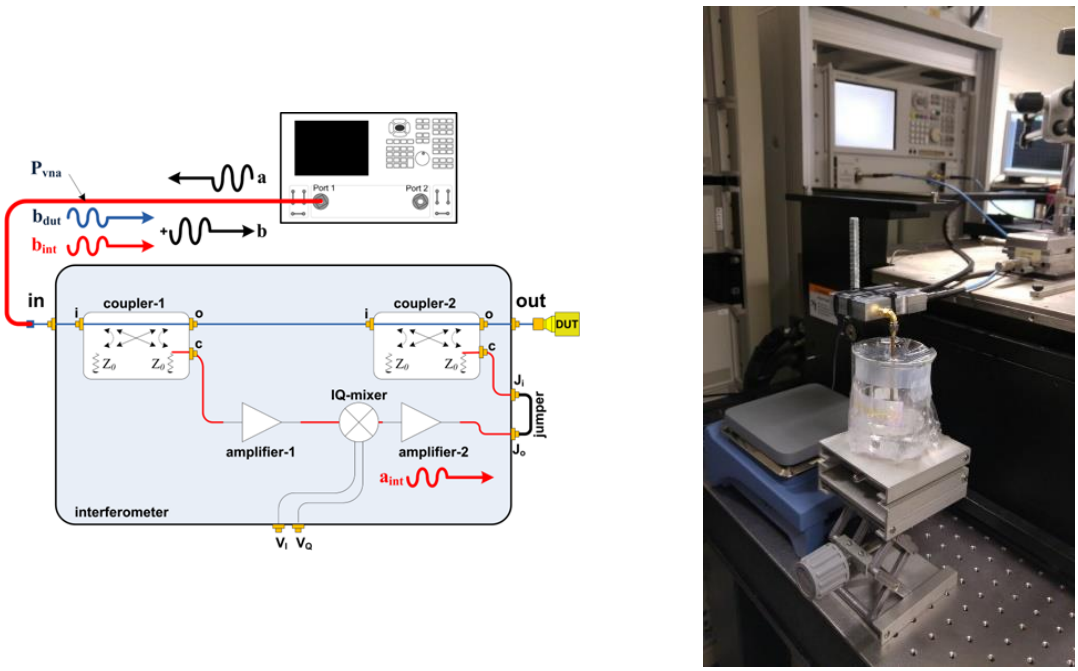

Figure 41: Left: block-diagram of the new high-frequency interferometer utilizing IQ-mixer steering techniques for IQ-modulation of the a_{int}-wave to achieve optimal cancelation of the reflected b_{dut}-wave for all Γ_{dut} values. Right: employed setup.

First tests of this concept have been performed for measurement up to 4GHz, showing a reduction of the VNA noise propagated and thus an increased resolution, as shown in Figure 42.

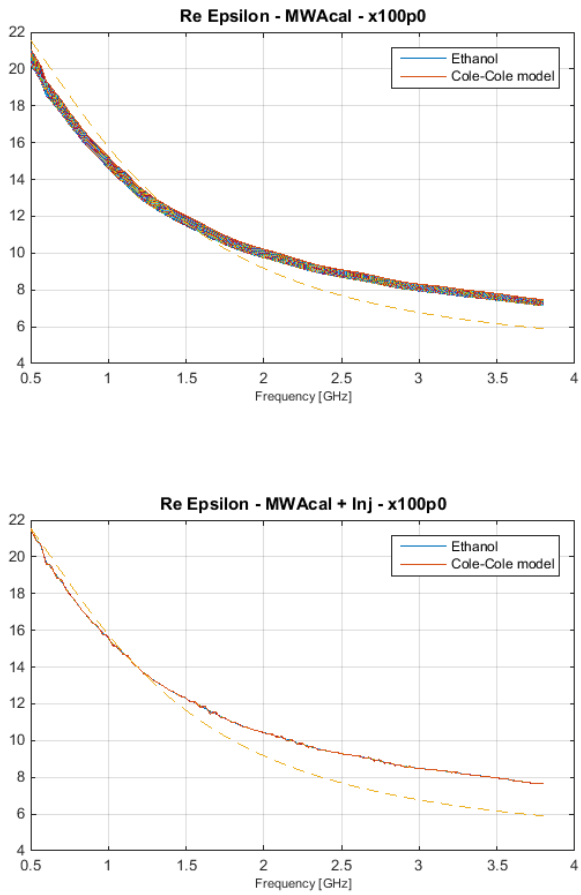

Figure 42: left: permittivity measurement with conventional VNA; right: permittivity measurement with interferometer VNA.

Current activities are based on employing a higher frequency interferometer, see Figure 43, for permittivity measurements up to 18GHz.

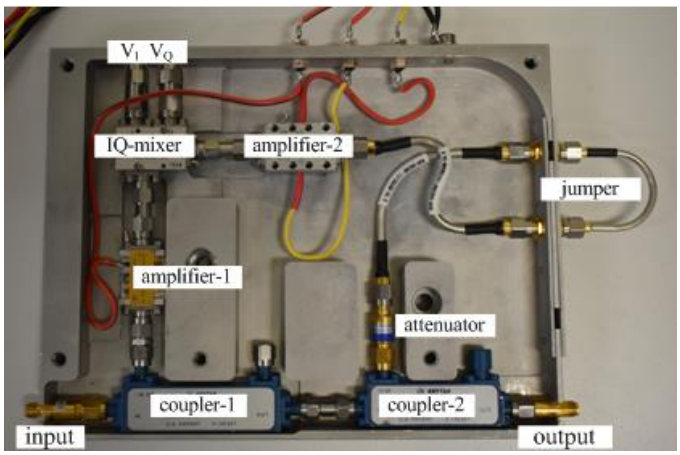

Figure 43: High-frequency (HF) interferometer module designed for the 2-18 GHz frequency range. The use of a passive IQ-mixer requires two additional amplifiers to compensate for losses.

6 Conclusion

This deliverable presented a description of the exposure systems to be used in the NextGEM project together with a thorough numerical and experimental dosimetry related to them, which allows the accurate estimation of the exposure conditions that will be used during bio-experiments. Well-established measurement techniques for materials characterization, as well as novel methods currently under investigation, have also been introduced that are relevant for correct dosimetry. A preliminary activity, preparatory for dosimetry related to the study on heavy and light mobile users to be carried out in Task 4.4 has also been shown.

Some exposure setups described in this deliverable have already been successfully employed for the experimental activities reported in Deliverables 4.3 and 4.4, while others will be employed within the Case Studies foreseen in the project. Since the activity of case studies has just started, some final adjustments and tunings could be necessary when the related experimental activities will start, and will be reported in the case studies-related deliverables.

The content of this deliverable represents a solid, technical ground for the high-quality experimental activities to be carried out in WP4 and in Case Studies envisaged in WP7.

7 References

[1] Schuderer, J., Samaras, T., Oesch, W., Spat, D., & Kuster, N. (2004). High peak SAR exposure unit with tight exposure and environmental control for in vitro experiments at 1800 MHz. IEEE Transactions on Microwave Theory and techniques, 52(8), 2057-2066.

[2] Jürgen Schuderer and Niels Kuster. Effect of the meniscus at the solid/liquid interface on the SAR distribution in Petri dishes and flasks. In: Bioelectromagnetics: Journal of the Bioelectromagnetics Society, The Society for Physical Regulation in Biology and Medicine, The European Bioelectromagnetics Association 24.2 (2003), pp. 103-108.

[3] Klarhofer M, B Csapo, C Balassy, JC Szeles and E Moser. (2001). High-resolution blood flow velocity measurements in the human finger. Magn Reson Med 45:716-9.

[4] Anna Sannino, Stefania Romeo, Maria Rosaria Scarfi, Daniele Pinchera, Fulvio Schettino, Mario Alonzo, Mariateresa Allocca, Olga Zeni, The effect of exposure to radiofrequency LTE signal and coexposure to mitomycin-C in Chinese hamster lung fibroblast V79 cells, Bioelectromagnetics 2023;1–12. DOI: 10.1002/bem.22478

[5] Falone, S., Sannino, A., Romeo, S., Zeni, O., Santini, S., Rispoli, R., Amicarelli, F., Scarfi, M.R.: Protective effect of 1950 MHz electromagnetic field in human neuroblastoma cells challenged with menadione. Sci. Rep. 8, 13234 (2018).

[6] M. L. Calabrese, G. d'Ambrosio, R. Massa, and G. Petraglia, "A high efficiency waveguide applicator for in vitro exposure of mammalian cells at 1.95 GHz," IEEE Trans. Microw. Theory Techn., vol. 54, no. 5, pp. 2256–2262, May 2006.

[7] A. Sannino, M. L. Calabrese, G. d'Ambrosio, R.Massa, G. Petraglia, P.Mita, M. Sarti, and M. R. Scarfi, "Evaluation of cytotoxic and genotoxic effects in human pheripheral blood leukocytes following exposure to 1950-MHz modulated signal," IEEE Trans. Plasma. Sci., vol. 34, no. 4, pp. 1441–1448, Aug. 2006.

[8] Stefania Romeo, Claudio D'Avino, Daniele Pinchera, Olga Zeni, Maria Rosaria Scarfi, Rita Massa, A waveguide applicator for in vitro exposures to single or multiple ICT frequencies, IEEE Trans. Microwave Theory and Techniques, Vol. 61, No. 5, May 2013, pp: 1994-2004 DOI: 10.1109/TMTT.2013.2246185.

[9] Eltiti, S., Wallace, D., Ridgewell, A., Zougkou, K., Russo, R., Sepulveda, F., Mirshekar-Syahkal, D., Rasor, P., Deeble, R., & Fox, E. (2007). Does short-term exposure to mobile phone base station signals increase symptoms in individuals who report sensitivity to electromagnetic fields? A double-blind randomized provocation study. Environmental health perspectives, 115(11), 1603–1608. https://doi.org/10.1289/ehp.10286

[10] Hill, D. A. (2009). Electromagnetic fields in cavities: deterministic and statistical theories. John Wiley & Sons.

[11] Dunlap, C. R., Holloway, C. L., Pirkl, R., Ladbury, J., Kuester, E. F., Hill, D. A., & Van de Beek, S. (2012, August). Characterizing reverberation chambers by measurements of the enhanced backscatter coefficient. In 2012 IEEE International Symposium on Electromagnetic Compatibility (pp. 210-215). IEEE.

[12] Fall, A. K., Besnier, P., Lemoine, C., Zhadobov, M., & Sauleau, R. (2014). Design and experimental validation of a mode-stirred reverberation chamber at millimeter waves. IEEE Transactions on Electromagnetic Compatibility, 57(1), 12-21.

[13] Holloway, C. L., Hill, D. A., Ladbury, J. M., & Koepke, G. (2006). Requirements for an effective reverberation chamber: Unloaded or loaded. IEEE Transactions on Electromagnetic Compatibility, 48(1), 187-194.

[14] Lucido, M., Massa, R., Panariello, G., & Schettino, F. (2022, May). Full-wave Validation of Plane Waves Model for Numerical Dosimetry in Reverberation Chambers. In 2022 Microwave Mediterranean Symposium (MMS) (pp. 1-4). IEEE.

[15] Vanden Abeele, M., Beullens, K., & Roe, K. (2013). Measuring mobile phone use: Gender, age and real usage level in relation to the accuracy and validity of self-reported mobile phone use. Mobile Media & Communication, 1(2), 213-236.

[16] International Electrotechnical Commission. (2016). Measurement procedure for the assessment of specific absorption rate of human exposure to radio frequency fields from hand-held and body-mounted wireless communication devices–Part 1: Devices used next to the ear (Frequency range of 300 MHz to 6 GHz). Geneva, Switzerland: IEC.

[17] Metaxas, A. C. (1996). Foundations of electroheat. A unified approach. In Fuel and Energy Abstracts (Vol. 3, No. 37, p. 193).

[18] Baker-Jarvis, J., Janezic, M. D., Grosvenor Jr, J. H., & Geyer, R. G. (1993). Transmission/reflection and short-circuit line methods for measuring permittivity and permeability. National Institute of Standards and Technology, NIST Technical Note 1355-R, pp 1-236.

[19] Anderson, J. M., Sibbald, C. L., & Stuchly, S. S. (1994). Dielectric measurements using a rational function model. IEEE transactions on microwave theory and techniques, 42(2), 199-204.
[20] Misra, D., Chabbra, M., Epstein, B. R., Microtznik, M., & Foster, K. R. (1990). Noninvasive electrical characterization of materials at microwave frequencies using an open-ended coaxial line: Test of an improved calibration technique. IEEE transactions on microwave theory and techniques, 38(1), 8-14.
[21] Migliore, M. D. (2000). Partial self-calibration method for permittivity measurement using truncated coaxial cable. Electronics Letters, 36(15), 1.
[22] Panariello, G., Verolino, L., & Vitolo, G. (2001). Efficient and accurate full-wave analysis of the open-ended coaxial cable. IEEE Transactions on Microwave Theory and Techniques, 49(7), 1304-1309.
[23] Romeo, S., Di Donato, L., Bucci, O. M., Catapano, I., Crocco, L., Scarfi, M. R., & Massa, R. (2011). Dielectric characterization study of liquid-based materials for mimicking breast tissues. Microwave and Optical Technology Letters, 53(6), 1276-1280.
[24] Stuchly, S. S., Sibbald, C. L., & Anderson, J. M. (1994). A new aperture admittance model for open-ended waveguides. IEEE transactions on microwave theory and techniques, 42(2), 192-198.
[25] Collin, R. E. (2007). Foundations for microwave engineering. John Wiley & Sons.
[26] Mubarak, F. A., Romano, R., Rietveld, G., & Spirito, M. (2020). A novel calibration method for active interferometer-based VNAs. IEEE Microwave and Wireless Components Letters, 30(8), 829-832.